Revision 1

Optical absorption anisotropy of high-density, wide-gap, high-hardness SiO_2 polymorphs *seifertite*, *stishovite* and *coesite*.

K. Klier[a], J.A. Spirko[b] and K. M. Landskron[a]

[a] Department of Chemistry, Lehigh University, E. Packer Ave, Bethlehem, PA 18015

[b] Department of Physical and Environmental Sciences, Texas A&M University-Corpus Christi, 6300 Ocean Dr, Unit 5802, Corpus Christi, TX 78414-5802

KEYWORDS: Theory, silica polymorphs, seifertite, stishovite, coesite, rutile, band structure, effective mass, optical absorption

ABSTRACT

Dense, high-refractive index, ultra-hard, wide-gap polymorphs of SiO_2, recently discovered orthorhombic *seifertite* (space group 60 Pbcn), and earlier characterized tetragonal *stishovite* (space group 136 P42/mnm) and monoclinic *coesite* (space group 15

C2/c) were studied using advanced methods of electronic structure calculations involving full-potential linearized augmented plane wave density functional theoretical method (FP-LAPW-DFT) with spin polarization, orbital dependent potentials, and modified Becke-Johnson potential (mBJ) for accurate account of the band gaps. Even though these calculations yield an excellent account of many properties, we here focus on quantitative aspects of optical absorption and selection rules therein. Specifically, the valence-to-conduction band transition in *seifertite* is symmetry-allowed, and is symmetry-forbidden in *stishovite* and *coesite*. Theory is compared with published experimental data, and explanation is provided for weak pre-edge optical absorption in *stishovite*. Electronic structure and calculated properties of *stishovite* are also compared with those of the isostructural *rutile* TiO_2. Effective masses are calculated from the energy dispersion curves $E(\mathbf{k})$ at the valence band maximum for holes and conduction band minimum for electrons. In addition, we propose that splitting of the O2p valence-band in *coesite* and also observed in *α-quartz* is a general feature of polymorphs with tetrahedrally coordinated Si, in contrast with continuous valence bands in those with octahedral SiO_6 units such as *seifertite* and *stishovite*. Based on quantitative results obtained from the BVA theory, this difference originates from a high degree of covalence in the tetrahedral polymorphs as opposed to high iconicity in octahedral polymorphs.

I. INTRODUCTION

Dense, high-refractive index, ultra-hard, wide-gap polymorphs of SiO_2 are of a great interest not only owing to the history of discovery in extraterrestrial matter and their extraordinary physical properties, but also to the underlying chemical bonding and unusual coordination of the Si-O_n structure-forming units and their arrangements. The most recently discovered and characterized polymorph of this type is orthorhombic *seifertite* (space group 60 Pbcn) (Dera et al. 2002; El Goresy et al. 2008), after tetragonal *stishovite* (space group 136 P42/mnm) was first synthesized in laboratory by Stishov and Popova (1961) and reported on its natural occurrence in Arizona meteor crater by Chao et al. (1962). The monoclinic *coesite* (space group 15 C2/c) was first synthesized by Coes (1953), its natural occurrence reported by Chao et al. (1960) and crystal structure determined by Levien and Prewitt (1981) and Smyth et al. (1987). Some of the experimentally determined properties of the investigated silicas as well as of selected reference materials are summarized in Table 1.

Table 1

The importance of these materials goes beyond their pure forms, especially as they serve as matrices holding impurities which impart on them new properties, both in nature and technology. For example, the exchange of $4H^+$ for Si^{4+}, "the hydrogarnet substitution", is considered to be one of the mechanisms for hydrogen storage in the deep Earth, *stishovite* being one of the vehicles for this storage as reported by Pawley et al. (1993), Williams and Hemley (2001), the crystal structure of synthetic H-bearing aluminous *stishovite*

having been reported by Smyth et al. (1995). Related to technology, diffusion of Cu^{+} in *α-cristobalite* was studied theoretically for possible implications to the functioning of nanoelectronic devices by Zelený et al. (2012), prompting an interest in general interaction of metals with the silica polymorphs. To advance the understanding of metal-support interactions at surfaces related to adhesion and catalysis, strength of bonding and agglomeration of Co and Ni on silica surfaces have been examined theoretically by Ma et al. (2000), (2001a), compared with those on alumina support by Ma et al. (2001b), and analyzed for periodic trends in interactions of the entire first-row transition metal series with the silica surface by Ma et al. (2002) on a slab model derived from *β-cristobalite*, using methods similar to those employed here, albeit focusing only on the ground-state properties.

Theory has now advanced to a level of high reliability and accuracy to attack both the fundamentals of electronic structure of pure crystalline materials such as the silicas considered here, and the effects of impurities and deliberately added dopants on properties such as optical spectra, luminescence, and carrier transport phenomena. While electronic structure of *stishovite* and *coesite* has been addressed in numerous papers (Xu and Ching 1991; Rudra and Fowler 1983), the most recently characterized *seifertite* has not so far to our knowledge been subject to theoretical analysis. Experimental optical absorption spectra of *stishovite* and *coesite*, but not *seifertite*, have also been reported by Trukhin et al. (2004). In this work, we present calculations of all three high-pressure polymorphs utilizing the full-potential linearized augmented plane wave (FP-LAPW) method as described by Singh (1994a) and implemented by Blaha et al. (2013) with the

86 modified Becke-Johnson (mBJ) potential of Tran and Blaha (2009) that is suited for
87 analysis of the entire electronic structure including core levels, valence and conduction
88 bands involving both oxygen and silicon orbitals, accurate band gaps, and core-level
89 shifts (CLS) for interpretation of photoelectron spectra. Because *stishovite* is
90 isostructural with TiO_2 *rutile*, we also compare their calculated properties and point out
91 the differences in bandgaps, optical transitions and carrier effective masses due to Ti ↔
92 Si replacement. Reliability of the present FP-LAPW-mBJ method is tested by a
93 comparison with experiment of Garvie et al (2000) and with published calculations
94 employing the GW quasiparticle approximation for *α-quartz* by Chang et al. (2000).
95 Optical absorption spectra are calculated in the single-particle approximation of
96 Ambrosch-Draxl and Sofo (2006), and spin-orbit interaction, although very small in the
97 materials studied, is also assessed using the second variational method as implemented by
98 Novák (2001). The present theoretical results may be considered as a background, or a
99 first stage, for the interpretation of experimental absorption spectra, as previously done
100 for amorphous SiO_2 using temperature dependence of Kramers-Kronig derived
101 absorption spectra in a recent study of Vella et al. (2011), as well as with theoretical
102 treatments of excitons in the pure and impurity-containing materials of this type,
103 employing methods already used for other SiO_2 polymorphs: amorphous silica modeled
104 as *β-cristobalite* by Laughlin (1980), *α-quartz* SiO_2 and TiO_2 using the Bethe-Salpeter
105 equation (BSE) employed by Lawler et al. (2008) and Kang and Hybertsen (2010), and *β-*
106 *cristobalite* with quasi-particle corrections to the Kohn-Sham eigenvalues determined by
107 the GW approximation used by Ramos et al. (2004).
108

II. SEMI-EMPIRICAL ASSESSMENT OF BOND STRENGTHS, COVALENCE AND IONICITY

An initial assessment of bonding and physical properties is motivated by the expediency of semi-empirical methods for a large number of compounds, herein with emphasis on the relation between known structures and degree of iconicity and covalence of the silica polymorphs studied. While ionic compounds are stabilized by long-range electrostatic [Madelung] interactions, covalent solids owe their stability to local bond strengths. The silica polymorphs are expected to be an intermediate case, i.e. compounds that are partially ionic and partially covalent. Presently we focus on the relation between structures with octahedral and tetrahedral coordination of nearest-neighbor oxygen atoms to Si and partial ionicity of the Si-O and Ti-O bonds. The simple semi-empirical analysis presented here leads to a clear distinction between the more ionic, octahedrally coordinated, and more covalent, tetrahedrally coordinated polymorphs.

One of the widely used semi-empirical analysis, cast in quantitative terms as the Bond-Valence (BVA) theory summarized and reviewed in the recent book by Brown (2002), is employed here in view of its great success in assaying the structure - bond strength relationships for a large number of inorganic compounds as documented e.g. by Brese and O'Keeffe (1991). Focusing on the MO_2 oxides (M = Si, Ti), hexa- and tetra-coordination of M atoms is linked to the ionicity or covalence of the M-O bond through the bond strength as defined in the BVA method. The key relationship between bond

131 strength S and the M-O bond length R is formulated in terms of two empirical parameters,
132 the length R_0 for a "reference" unit bond strength $S_{ref} = 1$ and a gauge parameter b, as
133
134 $$S = \exp[(R_0 - R)/b] \qquad \text{(II-1)}.$$
135
136 In the present work, we used values $R_0 = 1.624$ Å for Si and 1.815 Å for Ti, and $b = 0.37$
137 Å for both Si and Ti in Si-O and Ti-O bonds. An alternative three-parameter relationship
138
139 $$S = S_0 (R / R_0^{'})^{-N} \qquad \text{(II-2)},$$
140
141 may be adopted, with S_0, $R_0^{'}$ and N tabulated by Brown and Shannon (1973). For the
142 present oxides, we use $S_0 = 1.0$ valence units (v.u.) for Si, $S_0 = 0.666$ for Ti, $R_0^{'} = 1.625$ Å
143 for Si, $R_0^{'} = 1.952$ Å for Ti, and $N = 4.5$ for Si, $N = 4.0$ for Ti. This three-parameter bond-
144 valence relationship has also been recast by Brown and Shannon (1973) in terms of bond
145 covalence f_c as
146
147 $$f_c = aS^M \qquad \text{(II-3)},$$
148

where parameter values $a = 0.54$ for 10 core electrons in Si, $a = 0.49$ for 18 core electrons in Ti, and $M = 1.64$ for Si, $M = 1.57$ for Ti, are employed for the present MO_2 oxides. With these parameters, equation (II-3) yields practically identical results for S determined from either Eq. (II-1) or (II-2). In Table 2 we present results using crystallographic bond distances R for the Si-O and Ti-O bonds, parameters R_0 , b from Brown (2002), S calculated by (II-1), and covalence f_c calculated by (II-3) for the three silica polymorphs and TiO_2 *rutile*.

Table 2

Clearly, octahedrally coordinated Si or Ti oxides *seifertite*, *stishovite* and *rutile* are largely ionic (in average 70% ionic, or 30 % covalent), irrespective of whether the "cation" is Si or Ti, whereas those with tetrahedrally coordinated Si, *coesite* and *α-quartz*, are largely covalent (in average 40% ionic, or 60 % covalent). Results of this BVA analysis provide a powerful guidance for the interpretation of properties obtained from *ab initio* all-electron calculations in Section III ff. As an example, covalent character of the Si-O bonds in tetrahedral polymorphs results in an intrinsic gap in the valence band with split-off lower, largely covalent band (*viz*. Section IV-2, Fig. 4 and Appendix 2).

III. ELECTRONIC STRUCTURES AND OPTICAL TRANSITIONS FROM FIRST PRINCIPLES - METHODOLOGY

A full account for physical properties, including those of excited states involved in optical transitions, requires a theory that reaches beyond the semi-empirical relations described in Section II above. In the present work we employ a state-of-the-art quantum mechanical treatment specified in paragraphs III-1, III-2 and Appendix 1.

III-1. STRUCTURES AND RECIPROCAL LATTICE VECTORS

Structural data, reciprocal lattice vectors and their labeling used in the present study are given in Appendix 1. Graphic representations of the structures and reciprocal lattice vectors are in Figures A1-1 and A1-2 (*seifertite*), Figures A1-3 and A1-4 (*stishovite*), and Figures A1-5 and A1-6 (*coesite*).

III-2. COMPUTATIONAL METHOD

Electronic structure calculations presented herein involve full-potential linearized augmented plane wave density functional theoretical method (FP-LAPW-DFT) with spin polarization, orbital dependent potentials and modified Becke-Johnson potential (mBJ) for accurate account of the band gaps. For *α-quartz* as reference material, the mBJ bandgap (9.41 eV at the Γ point at the present level) and band structure was tested against experimental bandgap of 9.65 eV obtained from low-loss measurement in EELS/TEM by

Garvie et al. (2000) and compared with results of calculations using the GW approximation by Chang, Rohlfing and Louie (2000) resulting in the bandgap of 10.1 eV. Details of this test are summarized in Appendix 2, wherein the two sets of calculations are shown to be in a good agreement over the entire $E(\mathbf{k})$ band structure (*viz*. Figs. A2-1 and A2-2).

Also employed in the present work was the self-interaction correction *via* implementation of the LDA+*U* method in the fully localized limit (FLL)[†] for calculating orbital-dependent potentials to ensure that possible strong electron correlation in the partially occupied excited Si 3d*-orbitals be taken into account. While the effects of such a strong electron correlation are found to be small in periodic SiO_2 crystals, electron localization around defects such as Si with adjacent oxygen vacancies, or Si in neighborhood of transition-metal ion impurities, should not be a priori excluded. Therefore the present approach is to be viewed as providing a background for future studies of value for understanding coloration and, in general, optical properties of the silica polymorphs containing such defects. The justification for exploration of the Si 3d* orbitals in crystal physics is founded in their known effects on chemical bonding and in the relatively low separation of the Si3p and Si3d levels in the atomic spectrum of Si, 5.87 eV, from Kramida et al. (2013), which falls within the bandgap energies of the studied oxides. In the present work the value of $U\text{eff} = U\text{-}J = 0.46$ Ry was used for the Si3d orbitals and, for comparison, 0.25 Ry for Ti3d orbitals in *rutile*. Spin-orbit interaction was also included using the second variational method (Singh 1994b) implemented in the Wien2k package by Novák (2001), aiming at the detection of level splitting near the valence band

maximum that is well known for elemental silicon (experimental 42.6 meV found by Yu et al. (1989) and 42 meV determined by our theoretical calculations). In another example of spin-orbit effects in oxides, the value of -20 meV is obtained at the present level for ZnO, in agreement in sign and roughly in value with earlier tight-binding calculations by Fu and Wu (2008). These agreements validate the present theory for spin-orbit coupling energies as small as a few millielectron volts, which may or may not compete with crystal-field splittings caused by deviations from idealized high-symmetry structures.

Furthermore, as one of the main goals of this work, optical properties were calculated using the optic program of the Wien2k package. The theoretical background of this program has been developed by Ambrosch-Draxl and Sofo (2006). Because the Wien2k package utilizes a dual basis set of spherical harmonics in non-overlapping atomic "muffin tin" spheres α (MT_α) and plane waves in interstitial space (I), the matrix elements of the quantum mechanical dipole moment operator $\vec{\mu} = \sum_i q_i \vec{r}_i$ over all particles *i* with charges q_i at positions $\vec{r}_i$ are combined as a sum of contributions from the atomic spheres MT_α and interstitial space I as

$$< n'\vec{k} \mid \vec{\mu} \mid n\vec{k} > \; = \sum_\alpha < n'\vec{k} \mid \vec{\mu} \mid n\vec{k} >_{\mathrm{MT}_\alpha} + < n'\vec{k} \mid \vec{\mu} \mid n\vec{k} >_I \;,$$

symmetrized into square momentum matrix elements for all band combinations for each $\vec{k}$-point, and evaluated over a large number of $\vec{k}$-points (in this work 1,000) to obtain joint density of states and, upon Kramers-Kronig transformation, real and imaginary

components of the dielectric tensor and absorption coefficient. Calculations were carried out in several stages: after initialization from the structures listed in Appendix 1, standard scf cycle with spin polarization was run to self-consistency within < 1 mRy/bohr in forces, < 10^{-4} Ry in energy and < 10^{-4} in charge convergence, followed by LDA+U to the same convergence limits, and mBJ calculations run to the same convergence limits without forces. The properties were rendered by the energy bandstructure and optic programs of the Wien2k package (Blaha et al. 2013).

IV. ELECTRONIC STRUCTURES AND OPTICAL TRANSITIONS FROM FIRST PRINCIPLES – RESULTS

Computational results are divided into sections describing bandgaps and selection rules for transitions (IV-1) and band structures and optical absorption spectra (IV-2) for the silica polymorphs studied, including a comparison of isostructural *stishovite* SiO_2 and *rutile* TiO_2. These results afford an accurate account for properties of the minerals studied, which justifies an extension of already reported experimental work, as well as provides an impetus for optical and XPS studies of newly discovered minerals.

IV-1. BAND GAPS AND SELECTION RULES FOR OPTICAL TRANSITIONS.

All three SiO_2 polymorphs studied exhibit direct bandgaps at the Γ-points of their respective Brillouin zones. The state symmetries near bandgap edges are briefly summarized in this paragraph to assist interpretation of band-to-gap transitions through the use of optical dipole selection rules, *cf.* Figure 1. Assignments of irreducible representation labels are enabled by an analysis of the output of the present calculations consistent with the International Tables for Crystallography (1992) for space groups and tables of properties of point groups by Koster, Dimmock, Wheeler and Statz (1963) for equivalent Mulliken symbols of irreducible representations at the Γ-point of the BZ. In addition, the interactive Birkbeck College University of London space group database (1997-1999) is found useful.

Figure 1

Figure 1. Band-to-band transitions at the Γ-points of the BZ at the direct gaps of (a) *seifertite* (using Mulliken irreducible representation labels of the D_{2h} group), (b) *stishovite* (D_{2h}) and (c) *coesite* (C_{2h}). Green (red) arrows mark electric dipole allowed (forbidden) transitions. Thick arrows represent transitions VBM ($E_F = 0$) → CBM which are allowed in *seifertite*, and forbidden in *stishovite* and *coesite*. The closely separated valence band levels in *coesite* are expanded for clarity. The symbol for the bottom of conduction band BCB is used interchangeably with CBM.

A. ***Seifertite***. The direct bandgap transition between the top of valence band maximum (VBM) and bottom of conduction band minimum (CBM) without spin-orbit coupling (SOC) has the irreducible representation (irrep) symmetry $G_4^- \rightarrow G_1^+$, or $B_{3u} \rightarrow A_g$ under the D_{2h} group, hence it is allowed by the B_{3u} x-component of the electric dipole vector. Further down from the VBM are states G_4^+ (or B_{3g}, a symmetric combination of O2py orbitals at -0.23 eV, leading to forbidden transition at the Γ-point), G_3^- (or B_{1u}, at -0.28 eV, activated for transition to the A_g state at CBM by the B_{1u} z-component of the electric dipole vector), and G_2^- (or B_{2u}, at -0.62 eV, activated for transition to the A_g state at CBM by the B_{2u} y-component of the electric dipole vector). These selection rules are illustrated in Figure 1(a) and optical absorption is represented in Section IV-2.

With SOC, the VBM → CBM transition becomes $G_5^- \rightarrow G_5^+$, or $E_{1/2u} \rightarrow E_{1/2g}$ and is spin and symmetry allowed. This selection rule is consistent with the rule obtained without SOC.

B. ***Stishovite***. The direct bandgap transition VBM → CBM without SOC is $G_3^+ \rightarrow G_1^+$, or $B_{1g} \rightarrow A_g$ under the D_{2h} group, hence it is symmetry and parity forbidden. Identification of the irreps and forbiddenness is identical with the conclusion of Rudra and Fowler (1983) based on a semiempirical tight-binding approximation. Further inspection of levels below the VBM and above CBM reveals irrep symmetries shown in Figure 1(b). Of those, transition G_2^-, G_4^- (VBM-1) → G_1^+ (CBM), or B_{3u}, $B_{2u} \rightarrow A_g$ is allowed by the B_{3u}, B_{2u} (x,y) components of electric dipole, transition G_3^- (VBM-2) →

298 G_1^+ (CBM), or $B_{1u} \rightarrow A_g$ is allowed by the B_{1u} (z) component of electric dipole, and
299 transitions from G_3^+ (VBM) to three levels above CBM are all forbidden. These
300 selection rules clearly explain optical absorption anisotropy of *stishovite* demonstrated in
301 Section IV-2.

302

303 With SOC, the VBM → CBM transition becomes $G_5^+ \rightarrow G_5^+$ or $E_{1/2g} \rightarrow E_{1/2g}$, and is spin
304 and symmetry forbidden, consistent with the rule obtained without SOC.

305

306 C. ***Coesite***. The direct bandgap transition VBM → CBM without SOC is $G_1^+ \rightarrow G_1^+$, or
307 $A_{1g} \rightarrow A_{1g}$ under the C_{2h} group, hence it is symmetry forbidden. Further inspection of
308 levels below the VBM and above CBM reveals irrep symmetries shown in Figure 1(c).
309 Of those, transitions G_1^- (VBM-1,2) → G_1^+ (CBM), or $A_u \rightarrow A_g$ are allowed by the A_u (z)
310 component of electric dipole, transition G_2^- (VBM-4) → G_1^+ (CBM), or $B_u \rightarrow A_{1g}$ is
311 allowed by the B_u (x or y) component of electric dipole. The first transition from G_3^+
312 (VBM) to levels above CBM, G_1^+ (VBM) → G_1^- (CBM+1), or $A_g \rightarrow A_u$ is allowed.
313 These results explain the small optical anisotropy of *coesite* reported in Section IV-2.

314

315 With SOC, the VBM → CBM transition becomes $\{G_3^+ + G_4^+\} \rightarrow \{G_3^+ + G_4^+\}$, or $\{1E_{1/2g}$
316 $+ 2E_{1/2g}\} \rightarrow \{1E_{1/2g} + 2E_{1/2g}\}$, and is parity forbidden. This rule is consistent with the
317 forbiddenness obtained without SOC.

318

D. ***Rutile***. Here we give a brief summary of calculations of electronic structure of *rutile* TiO_2 with which *stishovite* is isostructural, however with empty Ti3d levels inside the large bandgap of 10 eV similar to that in *stishovite*. In addition, the *rutile* bandgap is indirect from the Γ to M point. This result agrees with calculations of Ekuma and Bagaoyko (2011). The presently calculated Γ → M bandgap of 3.12 eV is in a good agreement with that of Ekuma and Bagayoko and experimental values summarized therein. The direct gap Γ → Γ, 3.13 eV, is only by 10^{-2} eV larger, also in agreement with the results of Ekuma and Bagayoko (2011).

IV-2. BAND STRUCTURES, ENERGY DISPERSION IN THE MOMENTUM SPACE, AND OPTICAL ABSORPTION

We focus on several important features of the electronic structure of the silica polymorphs studied: the nature and symmetry of orbitals at the band edges, bandgaps, effective masses from curvatures of the energy dispersion, and intensities of optical absorption in different crystallographic directions that result in various degrees of optical anisotropy. These properties are derived from calculated band structures and optical absorptions of the three silica polymorphs and are shown in Figure 2 (*seifertite*), Figure 3 (*stishovite*), and Figure 4 (*coesite*). Electronic structure of TiO_2 *rutile* is presented in Figure 5, and its optical absorption is also shown in Figure 3 to demonstrate a substantial difference with the isostructural *stishovite*.

Figure 2

Figure 3

The band structure and optical absorption in *coesite* with tetrahedrally coordinated SiO_4 unit, represented in Figure 4, is substantially different from those in octahedrally coordinated SiO_6 units of *seifertite* and *stishovite*. In particular, we note the intrinsic gap within the O2p valence band, and a significant contribution of the off-diagonal component of absorption tensor (Abs-xz) and the low pre-edge absorption intensity at 8.5 – 10 eV due to forbidden band-to-band transition.

Figure 4

The *rutile* band structure calculated at the present level agrees well with the literature cited in Ekuma and Bagayoko (2011). Figure 5 shows the band structure of TiO_2 with O2p and Ti3d orbital contributions to the VB and the empty Ti^{4+} 3d intra-gap excited

361 levels located within a gap of 10.1 eV which, although larger, resembles that of *stishovite*
362 (Fig. 3) in terms of dispersion at the Γ-point edges of TBM and BCM.

363

364 Figure 5

365

366 Relations between band characters and splitting of the VB into two, separated by an
367 intrinsic gap that appears in the tetrahedrally coordinated Si in *coesite* (Figure 4) and *α-*
368 *quartz* (Figures A2-1 and A2-2 in Appendix 2), are also evident from partial DOS
369 analysis presented in Appendix 3, Figures A3-1 (*coesite*) and A3-2 (*α-quartz*). These VB
370 gaps in the tetrahedral polymorphs are in a marked contrast with the continuous VB of
371 the octahedrally coordinated Si, also evident from partial DOS in Appendix 3, Figures
372 A3-3 (*stishovite*) and A3-4 (*seifertite*).

373

374 V. DISCUSSION

375

376 *General comments.* The role of theory is seen not only in interpretation of experimental
377 data, but also in advancing powerful concepts that govern macroscopic physical
378 properties, relative stability of crystal structures, phase transformations, electronic and
379 optical phenomena, defect structure and reactivity of matter occurring in nature as well as
380 useful in man-made technologies. Theory also aims at the interpretation and derivation
381 of those relationships that have so far been empirical. An initial assessment of partial

382 iconicity/covalency is obtained with the use of simple and powerful semi-empirical
383 method derived from the constructs of Linus Pauling in the 1920s to 1940s, as widely
384 acknowledged by Brown (2002) and many others. This method, the bond-valence theory
385 (BVA), has led to a clear-cut distinction between more ionic, octahedrally coordinated
386 M-O_6 and more covalent, tetrahetrally coordinated M-O_4 compounds (M = Si, Ti), as
387 described in Section II. The subsequent quantum theory outlined in Sections III
388 (methodology) and IV (results) has the main strength in accounting for spectroscopic
389 properties which are beyond the range and focus of the BVA method. The present state-
390 of-the art quantum mechanical method, its validation and results are briefly described
391 below.

392

393 *The DFT method for wide-gap insulators.* In the present work, we have investigated
394 high-hardness, wide-gap silica polymorphs, inspired by our ongoing experimental effort
395 to achieve their synthesis at low pressures (Mohanty, Li, Liu, Fei and Landskron 2009)
396 and by questions regarding their optical properties, including those of the so far
397 theoretically unexplored *seifertite*. The presently employed method is the density
398 functional theory (DFT) of periodic systems that has proven highly successful in
399 describing ground state properties of crystals but had been found significantly lacking in
400 accuracy for excited states. However, an intensive development of several decades has
401 led to extensions of the theory that resulted in a substantially improved account for
402 important properties such as bandgap energies and optical transitions, including their
403 selection rules and anisotropies investigated herein. Of necessity, such extensions are
404 approximate and require a thorough validation, usually tested on reference compounds

with well-known properties. Also useful are comparisons of various levels of theory and approximations in terms of their relative merit. Furthermore, a successfully tested theory may be used for making predictions and designing future experiments. Herein we briefly describe the development of understanding the abovementioned properties of the silica polymorphs investigated in this work.

Validation of theoretical approximations. Results of the present level of theory (DFT-LAPW with LDA+*U* and mBJ potential) for the bandgap and $E(\mathbf{k})$ dispersion compare favorably with the quasi-particle Green's Wavefunction approximation (GW): The bandgap energy of *α-quartz* is found to be 9.41 eV by present method, 10.1 eV by GW, and from experiment 9.65 eV, as shown in Appendix 2. Thus *α-quartz* is considered a suitable test material for compositional silica polymorphs in terms of the choice of the mBJ potential and the Hubbard parameter *U*. Furthermore, a wide agreement among various theoretical methods and experiment on bandgap energy and $E(\mathbf{k})$ dispersion of TiO_2 *rutile* adds to the credibility of theory for the structural class of compounds which includes the presently investigated *stishovite*. And, given successful validation tests for *stishovite*, *coesite* and TiO_2 *rutile*, the new mBJ/LDA+*U* results for *seifertite* presented here are expected to be equally reliable.

Ionicity, covalence and intra-VB gap. On the molecular, atomic and ionic level, the silicas include the common polymorphs with tetra-coordinated building blocks SiO_4 and the high-pressure polymorphs with hexa-coordinated SiO_6 units. Based on these local

427 structural differences, a standard chemical argument as well as calculations using the
428 empirical BVA method (*cf.* Section II) would place the tetrahedral polymorphs among
429 compounds with stronger covalent bonds, while the six-fold coordination would indicate
430 prevalent ionic bonding. Indeed, one of the early tight-binding models by Rudra and
431 Fowler (1983) has successfully interpreted the VB structure of *stishovite* on the
432 assumption of a purely O2p ionic framework. The present work adds effects of Si orbitals
433 which merge into the lower portion of the VB but do not substantially change the VB $E(\mathbf{k})$
434 dispersion. This is consistent with low BVA covalence of 30% (or high 70% ionicity)
435 found for *stishovite* (Table 2 in Section II). Similarly, the octahedral SiO_6 building
436 blocks of *seifertite* are linked to high ionicity. In contrast, the high BVA covalence of 60%
437 in the tetrahedrally coordinated Si in *coesite* and *α-quartz* strongly suggests that purely
438 ionic model for the VB is insufficient, and therefore participation of covalent bonding
439 between the Si and O atoms through orbital overlaps and hybridization is necessary. This
440 is in fact revealed by the present quantum mechanical calculations that also elucidate the
441 structure-bonding relationships in the valence bands of the tetrahedral and octahedral
442 polymorphs.

443

444 While the VB of *seifertite*, *stishovite* and *rutile* are filled in a continuous manner (Figures
445 2, 3 and 5), *coesite* (Figure 4) exhibits an intrinsic gap similar to that in *α-quartz* as also
446 evident from band structures in Figures A2-1 and A2-3 of Appendix 2, and DOS plots
447 (Figures A3-4 and A3-5 of Appendix 3). The lack of the intrinsic gap within the valence
448 band is clearly an attribute of structures with octahedral coordination of Si (or Ti) by
449 nearest neighbor oxygen atoms, in contrast with the prevalence of such intrinsic gaps in

450 the more common tetrahedrally coordinated SiO_2 polymorphs. Across this "tetrahedral
451 polymorph" gap, the VB is split into a lower part, VB_{lower}, and upper part, VB_{upper}. A
452 qualitative explanation is in that VB_{lower} entails covalent Si-O bonding while VB_{upper} is
453 predominantly ionic. Quantum mechanical calculation of partial DOS for the Si and O
454 contributions (Appendix 3) confirms this expectation: The ratio of contributions from
455 atomic orbitals (AOs) in *coesite* AO(Si)/AO(O) is 0.34 in VB_{lower} and low 0.05 in VB_{upper}.
456 Moreover, AO(Si) and AO(O) completely overlap in VB_{lower} but not in VB_{upper}. Similar
457 condition governs the split VB in *α-quartz*, AO(Si)/AO(O) = 0.33 in VB_{lower} and 0.04 in
458 VB_{upper} .

459

460 *Optical transitions*. Calculated transitions represented in Figure 1 show allowed direct
461 transition for *seifertite*, and forbidden direct transition for *stishovite* and *coesite*. These
462 features, including anisotropies, are directly observable by optical measurements, which
463 as of this time are limited and lacking for *seifertite*. Present calculations predict that all
464 three SiO_2 polymorphs studied exhibit optical absorption anisotropy to various degrees.
465 The largest anisotropy of 1.5 eV is observed in *stishovite*, which is compared in Figure 3
466 with that of the isostructural *rutile* TiO_2 with the smallest degree of anisotropy.
467 Evidently substitution of Ti by Si results in both an increased bandgap and anisotropy
468 between the axial and equatorial directions: an analysis of orbital coefficients allows
469 identification of the lowest energy allowed transition as equatorial $O2p_{x,y} \rightarrow Si4s$ (B_{2u},
470 $B_{3u} \rightarrow A_g$). Calculated energy of this transition, 8.45 eV, is in a very good agreement
471 with the experimental value of 8.75 eV determined by Trukhin et al. (2004) using
472 *stishovite* single crystals. However, Trukhin et al. observed an additional weak transition

473 with a threshold of 7.6 eV, which these authors attributed to unspecified defects. Based
474 on the remarkable coincidence of the energy of this transition with the calculated
475 forbidden band-to-band transition (Figure 3), we suggest that this pre-edge weak
476 transition is actually native to perfect *stishovite* crystal due to the forbidden band-to-band
477 $B_{1g} \rightarrow A_{1g}$ transition at the Γ-point, whose forbiddenness is offset by nearby levels of
478 lower symmetry in the **k**-space. Inspection of Figure 3 for *stishovite* indeed shows the
479 onset of a weak transition with a threshold at 7.58 eV, close to the experimental value of
480 7.6 eV of Trukhin et al. (2004), which progresses to the onset of the main absorption
481 edge at 8.45 eV of the allowed B_{2u}, $B_{3u} \rightarrow A_{1g}$ transition. Calculations also predict a
482 second intense absorption edge at 10 eV, stimulated by z-polarized light, due to the $O2p_z$
483 → Si4s transition ($B_{1u} \rightarrow A_{1g}$ in Figure 3). This transition lies out of the experimental
484 range covered by Trukhin et al. (2004) and should be verified by an experiment reaching
485 into the 9-11 eV range. A comparison between calculated optical transitions between
486 *stishovite* and *rutile* (Figure 3) shows that such an anisotropy is suppressed in *rutile* TiO_2
487 due to close spacing of the $O2p_{x,y,z}$ levels near the TVB and different nature of the final
488 states at BCB, Si4s in *stishovite* and Ti3d in *rutile*.

489

490 Because of the importance of selection rules for optical transitions even in those cases
491 when the bandgap is direct, and the use of such rules for interpretation of observed
492 optical spectra, we present a graphic symmetry analysis of the nature of *stishovite* VBM
493 responsible for the forbidden transition across the direct VB → CB gap. In Figure 6 is
494 shown the B_{1g} orbital at the VB maximum, which causes the transition in *stishovite*
495 across the direct gap at the Γ-point to be forbidden.

Figure 6

Referring to Figure 6, we note that the Si s- or p-orbitals are not compatible with the B_{1g} symmetry, and the nearest possible "mixing in" Si orbital is $3d_{xy}$. Detailed analysis of partial charges in fact confirms the presence of such an admixture at the Γ-point, albeit small, on the order of 0.2% $Si3d_{xy}$, and of course zero contributions of the remaining Si3d orbitals with incompatible symmetry.

Effective masses. Band structure calculations contain information on effective masses of electrons and holes at the band edges, useful for assessing mobilities of current carriers injected into semiconducting or insulating compounds. Both intrinsic and external sources are considered for electron and hole injection. In this work, we present values of effective masses calculated from the curvatures $E(\mathbf{k})$ band structures at band edges as $m_{eff} = \left[\hbar^2 \Big/ \left(\partial^2 E \Big/ \partial k^2\right)_\Gamma\right]$. Results are summarized in Table 3.

Table 3

515 In all three silica polymorphs the bottom of the conduction band (conduction band
516 minimum - CBM) at the Γ-point is markedly dispersed, indicating significant mobility of
517 conduction electrons if injected. External source of injected conduction electrons could
518 employ surface-deposited Cs which was shown to transfer its 6s electron into a
519 chalcogenide lattice with near-100% efficiency by Park et al. (1996). The top of the
520 valence bands (valence band maximum - VBM) exhibits heavy character of holes if
521 injected, except in *seifertite* in which some mobility of conduction holes is indicated in
522 the x-direction. Data for *rutile* TiO_2 are also given for comparison with the isostructural
523 *stishovite*. Effective masses in the Ti3d CBM and O2p VBM are high, indicating low
524 mobility of the current carriers compared to *stishovite*.

525

526 VI. IMPLICATIONS

527

528 Among the many silica polymorphs, *seifertite* and *stishovite* are unique in their structure-
529 property relationships linked to the six-coordination of Si: high density, ultra-hardness,
530 optical absorption, and valence. The optical anisotropy revealed by the present theory
531 affords an observational tool for the detection of particles of these minerals in polarized
532 light and appropriately chosen energy ranges of the probing far-UV radiation.
533 Furthermore, valence-band XPS will readily distinguish between octahedrally and
534 tetrahedrally coordinated Si in the SiO_2 polymorphs, as well as in the more complex
535 compositions such as the $MgSiO_3$ *ilmenite*. As in the case of many useful connections
536 between the mineral world and man-made technology ranging from artificial gems to

lasers (as in ruby) to catalysts (as in zeolites), it may be anticipated that the present high-density silica polymorphs will also find a number of practical applications. When synthesized at mild conditions from mesoporous and microporous precursors, these materials may be considered not only as cheap substitutes for diamond in cutting tools and abrasives, but also as novel wide-gap insulators and semiconductors for optoelectronics and lasers. The present study yields results regarding properties of perfect crystals, which provide an incentive for experimental investigation of far-UV optical absorption and excitons, and for combined theoretical and experimental studies of intrinsic electronic defects such as oxygen vacancies, hydrogen, Cu, and Al or Ti substituted for Si. In particular, Ti substitution can be achieved by using microporous precursors such as the Ti-1 zeolite recently studied by Wells et al. (2004). Low effective masses and consequent high mobilities calculated for the conduction band edge hold promise for achieving n-conductivity upon appropriate doping with donors such as Zn and interstitial hydrogen.

Furthermore, since most occurring forms of these polymorphs are nanocrystalline, surface properties become important for their stability through termination of structure *e.g.* with hydroxyls for control of hydrophobic/hydrophilic properties, bioactivity in particle-cell interactions, external dopability by donors/acceptors for charge transfer, and electronic effects at interfaces with metals, semiconductors and organic matter in devices such as thin-film transistors, lasers and LEDs.

559 ACKNOWLEDGMENTS

560

561 The authors acknowledge grants of computational time and resources from the
562 Brookhaven National Laboratory – Center for Functional Nanomaterials, grant 30789
563 "Computational Studies in Support of Display Technology and Experimental Interface
564 Science" and from Lehigh University High-Performance Computing facility. They are
565 indebted to Professor W. Beall Fowler for insightful discussions on the theory of
566 electronic and optical properties of the oxide materials and to Professor Miltiadis K.
567 Hatalis for guiding applications of oxides for nano-electronics in Lehigh University's
568 Display Lab. A note from a referee regarding the Full Localized Limit (FLL) of the self-
569 interaction correction as implemented in the Wien2k package (*viz*. (FLL)† in Section III-
570 2), and his pointing out to the relevant discussion by Liechtenstein, Anisimov and Zaanen
571 (1995) is highly appreciated.

572

573 VII. REFERENCES

574

575 Ambrosch-Draxl, C., and Sofo, J.O. (2006) Linear optical properties of solids within the
576 full-potential linearized augmented planewave method. Computer Physics
577 Communications 175, 1-14.

578

579 Birkbeck College University of London (1997-1999)

580 Crystallographic Space Group Diagrams and Tables

581 http://img.chem.ucl.ac.uk/sgp/mainmenu.htm.

582

583 Blaha, P., Schwarz, K., Madsen, G.K.H., Kwasnicka, D., and Luitz, J. (2013) WIEN2k –

584 An Augmented Plane Wave + Local Orbitals Program for Calculating Crystal Properties",

585 Edition Wien2k_13.1; ISBN 3-9501031-1-2.

586

587 Brese, N.E., and O'Keeffe, M. (1991) Acta Crystallographica B47, 192-197.

588 Brown, I.D., and Shannon, R.D. (1973) Empirical bond-strength-bond-length curves for

589 oxides. Acta Crystallographica A29, 266-282.

590

591 Brown, I.D. (2002) The Chemical Bond in Inorganic Chemistry: The bond valence model.

592 Oxford University Press.

593

594 Chang, E.K., Rohlfing, M., and Louie, S.G. (2000) Excitons and optical properties of a-

595 quartz. Physical Review Letters 85, 2613-2616.

596

597 Chao, E.C.T, Shoemaker, E.M., and Madsen, B.M. (1960) First Natural Occurrence of

598 Coesite. Science 132, 220–222.

Chao, E.C.T., Fahey, J.J., Littler, J., and Milton, D.J. (1962) Stishovite, SiO_2, a very high pressure new mineral from meteor crater, Arizona. Journal of Geophysical Research 67, 419-421.

Coes, L. Jr. (1953) A New Dense Crystalline Silica. Science 118, 131–132.

Dera, P., Prewitt, C.T., Boctor, N.Z., and Hemley, R.J. (2002) Characterization of a high-pressure phase of silica from the Martian meteorite Shergotty. American Mineralogist 87, 1018–1023.

El Goresy, A., Dera, P., Sharp, T.G., Prewitt, C.T., Chen, M., Dubrovinsky, L., Wopenka, B., Boctor, N.Z., and Hemley, R.J. (2008) Seifertite, a dense orthorhombic polymorph of silica from the Martian meteorites Shergotty and Zagami. European Journal of Mineralogy 20, 523–528.

Ekuma, C.E., and Bagayoko, D. (2011) Ab-initio Electronic and Structural Properties of Rutile Titanium Dioxide. Japanese Journal of Applied Physics 50, 101103.

Fu, J.Y., and Wu, M.W. (2008) Spin-orbit coupling in bulk ZnO and GaN. Journal of Applied Physics 104, 093712 [1 – 7].

620 Garvie, L.A.J., Rez, P., Alvarez, J.R., Buseck, P.R., CravenA,J., and Brydson, R. (2000)
621 Bonding in alpha-quartz (SiO_2): A view of the unoccupied states. American Mineralogist
622 85, 732-738.
623
624 Horiuchi, H., Hirano, M., Ito, E., and Matsui, Y. (1982) MgSiO3 (ilmenite-type) : single
625 crystal X-ray diffraction study. American Mineralogist 67, 788-793.
626
627 International Tables for Crystallography (1992).
628
629 Kang, W., and Hybertsen, M.S. (2010) Quasiparticle and optical properties of rutile and
630 anatase TiO2. Physical Review B 82, 085203-1 to 085203-11.
631
632 Kokalj, A. (2003) Computer graphics and graphical user interfaces as tools in simulations
633 of matter at the atomic scale. Computational Materials Science 28, 155-168. Code
634 available from http://www.xcrysden.org/.
635
636 Koster, G.F., Dimmock, J.O., Wheeler, R.G., and Statz, H. (1963) Properties of the
637 Thirty-Two Point Groups. MIT press, Cambridge, Massachussetts.
638

639 Kramida, A., Ralchemko, Yi., Reader, J., and NIST ASD Team (2013) NIST Atomic
640 Spectra Database – Energy Levels. http://physics.nist.gov/PhysRefData/ASD.

641

642 Laughlin, R.B. (1980) Optical absorption edge in SiO2. Physical Review B 22, 3021 –
643 3029.

644

645 Lawler, H.M., Rehr, J.J., Vila, F., Dalosto, S.D., Shirley, E.L., and Levine, Z.H. (2008)
646 Optical to UV spectra and birefringence of SiO2 and TiO2: First principles calculation
647 with excitonic effects. Physical Review B 78, 205108-1 to 205108-8.

648 Levien, L., and Prewitt, C.T. (1981) High-pressure crystal structure and compressibility
649 of coesite. American Mineralogist 66, 324-333.

650

651 Liechtenstein, A.I., Anisimov, V.I., and Zaanen, J. (1995) Density-functional theory and
652 strong interactions: Orbital ordering in Mott-Hubbard insulators. Phys. Rev. B 52,
653 R5467(R).

654

655 Ma, Q., Klier, K., Cheng, H., Mitchell, J.W., and Hayes, K.S. (2000) Interaction
656 between catalysts and support 1. Low coverage of Co and Ni on silica surface. Journal of
657 Physical Chemistry B 104**,** 10618-10626.

658

659 Ma, Q., Klier, K., Cheng, H., Mitchell, J.W., and Hayes, K.S. (2001a) Interaction
660 between catalyst and support 3. Metal agglomeration on the silica surface. Journal of
661 Physical Chemistry B 105**,** 9230-9238.

662

663 Ma, Q., Klier, K., Cheng, H., Mitchell, J.W., and Hayes, K.S. (2001b) Interaction
664 between catalysts and support 2. Low coverage of Co and Ni on alumina surface. Journal
665 of Physical Chemistry B 105, 2212-2221.

666

667 Ma, Q., Klier, K., Cheng, H., and Mitchell, J.W. (2002) Interaction between catalyst and
668 support. 4. Periodic trends and patterns in interactions of first-row transition metals with
669 the silica surface. Journal of Physical Chemistry B 106, 10121-10127.

670

671 Mohanty, P., Li, D., Liu, T., Fei, Y., and Landskron, K. (2009) Synthesis of stishovite
672 nanocrystals from periodic mesoporous silica. Journal of American Chemical Society 131,
673 2764.

674

675 Novák, P. (2001) in WIEN2k: "~/SRC/novak_lecture_on_ldaumatrixelements.ps" and
676 http://www.wien2k.at/reg_user/textbooks.

677

678 Park, K.T., Richards-Babb, M., Freund, M.S., Weiss, J., and Klier, K. (1996) Surface
679 structure of single crystal MoS_2 (0002) and Cs/MoS_2 (0002) by X-ray photoelectron
680 diffraction. Journal of Physical Chemistry 100, 10739-10745.

Pawley, A.R., McMillan, P.F., and Holloway, J.R. (1993) Hydrogen in Stishovite, with Implications for Mantle Water Content. Science 261, 1024-1026.

Ramos, L.E., Furtmueller, J., and Bechstedt, F. (2004) Quasiparticle band structures and optical spectra of b-cristobalite SiO2. Physical Review B 69, 085102-1 to 085102-8.

Rudra, J.K., and Fowler, W.B. (1983) Electronic band structure of stishovite (tetragonal SiO_2). Physical Review B 28, 1061-1087.

Singh, D.J. (1994a) Planewaves, Pseudopotentials, and the LAPW Method. Kluwer Academic Publishers Boston, Dordrecht, London.

Singh, D.J. (1994b) Planewaves, Pseudopotentials, and the LAPW Method, Kluwer Academic Publishers Boston, Dordrecht, London, pp.86-87.

Smyth, J.R., Smith, J.V., Artioli, G., and Kvick, Åke (1987) Crystal Structure of Coesite, a High-pressure Form of SiO_2, at 15 and 298 K from Single-Crystal Neutron and X-ray Dlffraction Data: Test of Bonding Models. Journal of Physical Chenistry 91, 988-992.

Smyth, J.R., Swope, R.J., and Pawley, A.R. (1995) H in rutile-type compounds: II. Crystal chemistry of Al substitution in H-bearing stishovite. American Mineralogist 80, 454-456.

Solovyev, I.V., Dederichs,P.H., and Anisimov, V.I. (1994) Corrected atomic limit in the local density approximation and the electronic structure of *d* impurities in Rb. Physical Review B 50, 16861 – 16871.

Stishov, S.M., and Popova, S.V. (1961) A new modification of silica. Geokhimiya 10, 837-839.

Tran, F., and Blaha, P. (2009) Accurate band gaps of semiconductors and insulators with a semilocal exchange-correlation potential. Physical Review Letters 102, 226401-1 - 226401-4.

Trukhin, A.N., Dyuzheva, T.I., Lityagina, L.M., and Bendeliani, N.A. (2004) Intrinsic absorption threshold of stishovite and coesite. Solid State Communications, 1–5.

Vella, E., Messina, F., Cannas, M., and Boscaino, R, (2011) Unraveling exciton dynamics in amorphous silicon dioxide: Interpretation of the optical features from 8 to 11 eV. Physical Review B 83, 174201-1 to 174201-8.

722 Weinberg, Z.A., Rubloff. G.W., and Bassous, E. (1979) Transmission, photoconductivity,
723 and the experimental band gap of thermally grown SiO_2 films. Physical Review B 19,
724 3107 – 3117.

725

726 Wells, D.H. Jr., Delgass, W.N., and Kendall T. Thomson,K.T. (2004) Evidence of
727 defect-promoted reactivity for epoxidation of propylene in titanosilicate (TS-1) catalysts:
728 A DFT study. Journal of American Chemical Society 126, 2956-2962.

729

730 Williams, Q., and Hemley, R.J. (2001) Hydrogen in the Deep Earth. Annual Review of
731 Earth Planetary Science 29, 365–418.

732

733 Xu, Y., and Ching, W.Y. (1991) Electronic and optical properties of all polymorphic
734 forms of silicon dioxide. Physical Review B 44, 11048-11058.

735

736 Yu, Z., Huang, Y.X., and Shen, S.C. (1989) Spin-orbit splitting of the valence bands in
737 silicon determined by means of high-resolution photoconductive spectroscopy. Physical
738 Review B 39, 6287–6289.

739

740 Zelený, M., Hegedüs, J., Foster, A.S., Drabold, D.A., Elliott, S.R., and Nieminen, R.M.
741 (2012) Ab initio study of Cu diffusion in α-cristobalite. New Journal of Physics 14,
742 113029.

743

744
745
746
747
748
749
750
751
752
753
754
755
756
757
758
759
760
761
762
763
764
765
766
767
768
769
770
771

772 **SUPPORTING DOCUMENTATION**

773

774 **APPENDIX 1 Structural data, reciprocal lattice vectors and their labeling for**

775 ***seifertite, stishovite, coesite* and *rutile* used in the present study.**

776

777 *a. Seifertite*

778

779 *Seifertite*, space group 60 Pbcn, has the structure shown in Figure A1-1.

780

781 Figure A1-1

782

783 Figure A1-1 Unit cell of *seifertite.* Values of primitive translations a, b, c in the x, y, z
784 directions and fractional coordinates of Si and O are given in the text. The coordination
785 of Si by O is nearly octahedral and that of O by Si is trigonal.

786

787 Lattice constants and fractional coordinates are from Dera et al. (2002).

788

789 The primitive translation vectors of its orthorhombic cell (***a,b,c***) ≡ (a $\hat{x}$, b $\hat{y}$, c $\hat{z}$) are

790

a = 7.742210 bohr,

b = 9.528000 bohr,

c = 8.493570 bohr,

The unit cell contains 4 SiO_2 formula units with 4 equivalent Si atoms and 8 O atoms at fractional coordinates of the unique atoms

Si (0.0000, 0.1522, 0.2500),

O (0.7336, 0.6245, 0.9186),

the rest being generated by the symmetry operations of the Pbcn group as in the Birkbeck College University of London (1997-1999) space group database. The space group Pb2n given by El Goresy et al. (2008) as an alternative was not used, since satisfactory results were obtained with the higher symmetry Pbcn group.

The reciprocal lattice is also orthorhombic, formed by the vectors (***a*, b*, c****) such that

$\boldsymbol{a}^* = 2\pi\,(\boldsymbol{b} \times \boldsymbol{c})/[\boldsymbol{a}.(\boldsymbol{b} \times \boldsymbol{c})] = 0.811549\ \hat{x}\ \text{bohr}^{-1}$,

$\boldsymbol{b}^* = 2\pi\,(\boldsymbol{c} \times \boldsymbol{a})/[\boldsymbol{a}.(\boldsymbol{b} \times \boldsymbol{c})] = 0.659444\ \hat{y}\ \text{bohr}^{-1}$,

$\boldsymbol{c^*} = 2\pi\ (\boldsymbol{a} \times \boldsymbol{b})/[\boldsymbol{a}.(\boldsymbol{b} \times \boldsymbol{c})] = 0.739758\ \hat{z}\ \text{bohr}^{-1}$

as shown in Figure A1-2.

Figure A1-2

Figure A1-2 Brillouin zone of the orthorhombic lattice. Critical points chosen for the band structure representation are labeled as Γ (0,0,0), Z (0,0, ½), R (½, ½, ½), S (½, ½,0), X (½,0,0), U (½,0, ½). Lengths of the reciprocal vectors a*, b*, c* are in the ratio generated by the *seifertite* structure.

b. <u>*Stishovite*</u>

Stishovite, space group 136 P42/mnm, has the structure shown in Figure A1-3.

Figure A1-3

Figure A1-3 Unit cell of *stishovite.* Values of primitive translations a, b, c in the x, y, z directions and fractional coordinates of Si and O are given in the text. The coordination of Si by O is nearly octahedral and that of O by Si is trigonal.

Lattice constants and fractional coordinates are from Rudra and Fowler (1983).

The primitive translation vectors of its tetragonal cell $(\boldsymbol{a,b,c}) \equiv (a\,\hat{x}, a\,\hat{y}, c\,\hat{z})$ are

a = 7.893770 bohr,

b = 7.893770 bohr,

c = 5.036310 bohr,

The unit cell contains 2 SiO_2 formula units with fractional coordinates of the Si and O atoms

Si (1) (0.0000, 0.0000, 0.0000),

Si (2) (0.5000, 0.5000, 0.5000),

O (3) (0.3062, 0.3062, 0.0000),

O (4) (0.6938, 0.6938, 0.0000),

O (5) (0.1938, 0.8062, 0.5000),

O (6) (0.8062, 0.1938, 0.5000),

generated from unique positions of Si(1) and O(3) by the symmetry operations of the P42/mnm group.

The reciprocal lattice is also tetragonal, formed by the vectors (***a*, b*, c****) such that

$\boldsymbol{a}^* = 2\pi\,(\boldsymbol{b} \times \boldsymbol{c})/[\boldsymbol{a}.(\boldsymbol{b} \times \boldsymbol{c})] = 0.795968\ \hat{x}\ \text{bohr}^{-1}$,

$\boldsymbol{b}^* = 2\pi\,(\boldsymbol{c} \times \boldsymbol{a})/[\boldsymbol{a}.(\boldsymbol{b} \times \boldsymbol{c})] = 0.795968\ \hat{y}\ \text{bohr}^{-1}$,

$\boldsymbol{c}^* = 2\pi\,(\boldsymbol{a} \times \boldsymbol{b})/[\boldsymbol{a}.(\boldsymbol{b} \times \boldsymbol{c})] = 1.247577\ \hat{z}\ \text{bohr}^{-1}$

shown in Figure A1-4 with labeling of the special points consistent with that that of Rudra and Fowler (1983).

Figure A1-4

Figure A1-4 Brillouin zone of the tetragonal lattice. Critical points chosen for the band structure representation are labeled as Γ (0,0,0), Z (0,0, ½), A (½, ½, ½), M (½, ½,0), X (½,0,0), R (½,0, ½). Intermediate points Λ, S, V, Σ, Δ, W and U have coordinates

865 specified in the klist_band for the tetragonal lattice. Lengths of the reciprocal vectors a*,
866 b*, c* are in the ratio yielded by the *stishovite* structure.

867

868

869 *c. Coesite*

870

871 *Coesite*, space group 15 C2/c, has the structure shown in Figure A1-5.

872

873 Figure A1-5

874

875 Figure A1-5 Unit cell of *coesite* as a stereo picture. Values of primitive translations a, b,
876 c in the x, y, z directions and fractional coordinates of Si and O are given in the text. The
877 coordination of Si by O is tetrahedral and that of O by Si is two-fold. O atoms at (0,0,0)
878 and (1/2,1/2,1/2) are linearly coordinated to the nearest two Si neighbors, a feature that
879 has influence on distribution of levels in the valence band.

880

881

882 Lattice constants and fractional coordinates are taken from single crystal neutron
883 diffraction data at 292 K by Smyth et al. (1987).

884

885 The primitive translation vectors of its monoclinic cell (***a,b,c***) ≡ (a $\hat{x}$, b $\hat{y}$, c1 $\hat{x}$ + c2 $\hat{z}$) are

886

887 a = 13.4845 bohr,

888 b = 23.4014 bohr,

889 c1 = -6.8665 bohr,

890 c2 =11.7154 bohr,

891

892 and the angle subtended by vectors ***a*** and ***c*** is $\beta = 120.375^{o}$.

893

894 The unit cell contains 16 SiO_2 formula units with two Si and five O unique atoms at

895 fractional coordinates

896

897 Si(1) (0.14032, 0.10832, 0.07231) multiplicity 4,

898 Si(2) (0.50677, 0.15800, 0.54073) multiplicity 4,

899 O(1) (0.00000, 0.00000, 0.00000) multiplicity 2,

900 O(2) (0.50000, 0.11643, 0.75000) multiplicity 2,

901 O(3) (0.26631, 0.12320, 0.94031) multiplicity 4,

902 O(4) (0.31144, 0.10379, 0.32785) multiplicity 4,

903 O(5) (0.01746, 0.21192, 0.47851) multiplicity 4,

904

905 the rest being generated by the symmetry operations of the C2/c group[29].

906

907 The reciprocal lattice is also monoclinic, formed by the vectors (***a*, b*, c****) such that

908

909 $\boldsymbol{a^*} = 2\pi\,(\boldsymbol{b} \times \boldsymbol{c})/[\boldsymbol{a}.(\boldsymbol{b} \times \boldsymbol{c})] = (0.465956\ \hat{x} + 0.273102\ \hat{z})\ \text{bohr}^{-1}$,

910 $\boldsymbol{b^*} = 2\pi\,(\boldsymbol{c} \times \boldsymbol{a})/[\boldsymbol{a}.(\boldsymbol{b} \times \boldsymbol{c})] = 0.268496\ \hat{y}\ \text{bohr}^{-1}$,

911 $\boldsymbol{c^*} = 2\pi\,(\boldsymbol{a} \times \boldsymbol{b})/[\boldsymbol{a}.(\boldsymbol{b} \times \boldsymbol{c})] = 0.536318\ \hat{z}\ \text{bohr}^{-1}$,

912

913 shown in Figure A1-6 with special points generated with the help of the Xcrysden
914 program, Kokalj (2003).

915 The angles between the reciprocal lattice vectors are $\sphericalangle(\boldsymbol{a^*}, \boldsymbol{c^*}) = 59.625^{o}$ and $\sphericalangle(\boldsymbol{a^*}, \boldsymbol{b^*}) =$
916 $\sphericalangle(\boldsymbol{b^*}, \boldsymbol{c^*}) = 90^{o}$. and lengths of the reciprocal vectors a*, b*, c* are in the ratio created
917 by the *coesite* structure. The coesite structure in this representation is close to hexagonal
918 about the principal axis ***b***.

919

920 Figure A1-6

921

922 Figure A1-6 Brillouin zone of the monoclinic, nearly hexagonal lattice about the b* axis.

Critical points chosen for the band structure representation are labeled as:

Γ (0,0,0), K2 (0, ½, 0), K3 (0.335, ½, 0.33), K4 (0.335,0, 0.33), K5 = Γ, K6 (½,0,0), K7 (½,½,0), K8 = K2.

The corresponding labels for the idealized hexagonal lattice are:

Γ ≡ [K1 = K5], A ≡ [K2 = K8], H ≡ K3, K ≡ K4, M ≡ K6 and L ≡ K7

Wien 2k structure files of *seifertite, stishovite, coesite* and *rutile*

Seifertite

```
P   LATTICE,NONEQUIV. ATOMS  2                        60 Pbcn
MODE OF CALC=RELA
  7.742210  9.528000  8.493570 90.000000 90.000000 90.000000
ATOM  -1: X=0.00000000 Y=0.15220000 Z=0.25000000
           MULT= 4          ISPLIT= 8
       -1: X=0.00000000 Y=0.84780000 Z=0.75000000
       -1: X=0.50000000 Y=0.65220000 Z=0.25000000
       -1: X=0.50000000 Y=0.34780000 Z=0.75000000
Si1        NPT=  781  R0=0.00010000 RMT=    1.6000   Z: 14.0
LOCAL ROT MATRIX:    0.0000000 1.0000000 0.0000000
                     0.0000000 0.0000000 1.0000000
```

```
                      1.0000000 0.0000000 0.0000000
ATOM  -2: X=0.73360000 Y=0.62450000 Z=0.91860000
           MULT= 8          ISPLIT= 8
       -2: X=0.26640000 Y=0.37550000 Z=0.08140000
       -2: X=0.23360000 Y=0.12450000 Z=0.58140000
       -2: X=0.76640000 Y=0.87550000 Z=0.41860000
       -2: X=0.76640000 Y=0.12450000 Z=0.91860000
       -2: X=0.23360000 Y=0.87550000 Z=0.08140000
       -2: X=0.26640000 Y=0.62450000 Z=0.58140000
       -2: X=0.73360000 Y=0.37550000 Z=0.41860000
O 2        NPT=  781  R0=0.00010000 RMT=    1.6000   Z:  8.0
LOCAL ROT MATRIX:    1.0000000 0.0000000 0.0000000
                     0.0000000 1.0000000 0.0000000
                     0.0000000 0.0000000 1.0000000
8 symmetry operations are auto-generated by the Pbcn group
-------------------------------------------------------------------------------------------------

***Stishovite***
P   LATTICE,NONEQUIV. ATOMS  2                  136 P42/mnm
MODE OF CALC=RELA
  7.893770  7.893770  5.036310 90.000000 90.000000 90.000000
```

```
ATOM  -1: X=0.00000000 Y=0.00000000 Z=0.00000000
           MULT= 2          ISPLIT= 8
       -1: X=0.50000000 Y=0.50000000 Z=0.50000000
Si         NPT=  781  R0=0.00010000 RMT=    1.6500   Z: 14.0
LOCAL ROT MATRIX:    0.7071068 0.7071068 0.0000000
                    -0.7071068 0.7071068 0.0000000
                     0.0000000 0.0000000 1.0000000
ATOM  -2: X=0.30620000 Y=0.30620000 Z=0.00000000
           MULT= 4          ISPLIT= 8
       -2: X=0.69380000 Y=0.69380000 Z=0.00000000
       -2: X=0.19380000 Y=0.80620000 Z=0.50000000
       -2: X=0.80620000 Y=0.19380000 Z=0.50000000
O 1        NPT=  781  R0=0.00010000 RMT=    1.6500   Z:  8.0
LOCAL ROT MATRIX:    0.0000000-0.7071068 0.7071068
                     0.0000000 0.7071068 0.7071068
                    -1.0000000 0.0000000 0.0000000

16 symmetry operations are auto-generated by the P42/mnm group

-------------------------------------------------------------------------
```

985 ***Coesite***

986 P LATTICE,NONEQUIV. ATOMS 7

987 MODE OF CALC=RELA

988 13.484500 23.401400 13.579400 90.000000120.375000 90.000000

989 ATOM -1: X=0.13998000 Y=0.10847000 Z=0.07211000

990 MULT= 4 ISPLIT= 8

991 -1: X=0.86002000 Y=0.89153000 Z=0.92789000

992 -1: X=0.86002000 Y=0.10847000 Z=0.42789000

993 -1: X=0.13998000 Y=0.89153000 Z=0.57211000

994 Si1 NPT= 781 R0=0.00010000 RMT= 1.4900 Z= 14.0

995 LOCAL ROT MATRIX: 1.0000000 0.0000000 0.0000000

996 0.0000000 1.0000000 0.0000000

997 0.0000000 0.0000000 1.0000000

998 ATOM -2: X=0.50722000 Y=0.15785000 Z=0.54153000

999 MULT= 4 ISPLIT= 8

1000 -2: X=0.49278000 Y=0.84215000 Z=0.45847000

1001 -2: X=0.49278000 Y=0.15785000 Z=0.95847000

1002 -2: X=0.50722000 Y=0.84215000 Z=0.04153000

1003 Si2 NPT= 781 R0=0.00010000 RMT= 1.4900 Z= 14.0

1004 LOCAL ROT MATRIX: 1.0000000 0.0000000 0.0000000

1005 0.0000000 1.0000000 0.0000000

```
                    0.0000000 0.0000000 1.0000000
ATOM  -3: X=0.00000000 Y=0.00000000 Z=0.00000000
          MULT= 2          ISPLIT= 8
      -3: X=0.00000000 Y=0.00000000 Z=0.50000000
O 1       NPT=  781  R0=0.00010000 RMT=    1.4900   Z=  8.0
LOCAL ROT MATRIX:    1.0000000 0.0000000 0.0000000
                    0.0000000 1.0000000 0.0000000
                    0.0000000 0.0000000 1.0000000
ATOM  -4: X=0.50000000 Y=0.11524000 Z=0.75000000
          MULT= 2          ISPLIT= 8
      -4: X=0.50000000 Y=0.88476000 Z=0.25000000
O 2       NPT=  781  R0=0.00010000 RMT=    1.4900   Z=  8.0
LOCAL ROT MATRIX:    0.0000000 1.0000000 0.0000000
                    0.0000000 0.0000000 1.0000000
                    1.0000000 0.0000000 0.0000000
ATOM  -5: X=0.26400000 Y=0.12452000 Z=0.93830000
          MULT= 4          ISPLIT= 8
      -5: X=0.73600000 Y=0.87548000 Z=0.06170000
      -5: X=0.73600000 Y=0.12452000 Z=0.56170000
      -5: X=0.26400000 Y=0.87548000 Z=0.43830000
O 3       NPT=  781  R0=0.00010000 RMT=    1.4900   Z=  8.0
```

```
LOCAL ROT MATRIX:    1.0000000 0.0000000 0.0000000
                     0.0000000 1.0000000 0.0000000
                     0.0000000 0.0000000 1.0000000
ATOM  -6: X=0.31277000 Y=0.10319000 Z=0.32768000
          MULT= 4          ISPLIT= 8
       -6: X=0.68723000 Y=0.89681000 Z=0.67232000
       -6: X=0.68723000 Y=0.10319000 Z=0.17232000
       -6: X=0.31277000 Y=0.89681000 Z=0.82768000
O 4        NPT=  781  R0=0.00010000 RMT=    1.4900   Z=  8.0
LOCAL ROT MATRIX:    1.0000000 0.0000000 0.0000000
                     0.0000000 1.0000000 0.0000000
                     0.0000000 0.0000000 1.0000000
ATOM  -7: X=0.01900000 Y=0.21178000 Z=0.47664000
          MULT= 4          ISPLIT= 8
       -7: X=0.98100000 Y=0.78822000 Z=0.52336000
       -7: X=0.98100000 Y=0.21178000 Z=0.02336000
       -7: X=0.01900000 Y=0.78822000 Z=0.97664000
O 5        NPT=  781  R0=0.00010000 RMT=    1.4900   Z=  8.0
LOCAL ROT MATRIX:    1.0000000 0.0000000 0.0000000
                     0.0000000 1.0000000 0.0000000
                     0.0000000 0.0000000 1.0000000
```

```
4 symmetry operations are auto-generated by the C2/c group
-------------------------------------------------------------------------------------------------
```

Rutile - lattice constants from Ekuma and Bagayoko (2011), fractional coordinates as in stishovite

```
P   LATTICE,NONEQUIV. ATOMS  2                    136 P42/mnm
MODE OF CALC=RELA
  8.683743  8.683743  5.593006 90.000000 90.000000 90.000000
ATOM  -1: X=0.00000000 Y=0.00000000 Z=0.00000000
           MULT= 2          ISPLIT= 8
       -1: X=0.50000000 Y=0.50000000 Z=0.50000000
Ti         NPT=  781  R0=0.00005000 RMT=    1.9000   Z: 22.0
LOCAL ROT MATRIX:    0.7071068 0.7071068 0.0000000
                    -0.7071068 0.7071068 0.0000000
                     0.0000000 0.0000000 1.0000000
ATOM  -2: X=0.30620000 Y=0.30620000 Z=0.00000000
           MULT= 4          ISPLIT= 8
       -2: X=0.69380000 Y=0.69380000 Z=0.00000000
       -2: X=0.19380000 Y=0.80620000 Z=0.50000000
       -2: X=0.80620000 Y=0.19380000 Z=0.50000000
```

```
O 1        NPT=  781  R0=0.00010000 RMT=    1.7000   Z:  8.0
LOCAL ROT MATRIX:    0.0000000-0.7071068 0.7071068
                     0.0000000 0.7071068 0.7071068
                    -1.0000000 0.0000000 0.0000000
16 symmetry operations are auto-generated by the P42/mnm group
```

List of k-points for band structure rendition of *seifertite*, *stishovite*, *coesite* and *rutile*

***Seifertite*:**

```
GAMMA          0    0    0   12  2.0-8.00 8.00
               0    0    1   12  2.0
               0    0    2   12  2.0
               0    0    3   12  2.0
               0    0    4   12  2.0
               0    0    5   12  2.0
Z              0    0    8   16  2.0
               1    1    8   16  2.0
               2    2    8   16  2.0
```

1089		3	3	8	16	2.0
1090		4	4	8	16	2.0
1091		5	5	8	16	2.0
1092		6	6	8	16	2.0
1093		7	7	8	16	2.0
1094	R	6	6	6	12	2.0
1095		6	6	5	12	2.0
1096		6	6	4	12	2.0
1097		6	6	3	12	2.0
1098		6	6	2	12	2.0
1099		6	6	1	12	2.0
1100	S	8	8	0	16	2.0
1101		7	7	0	16	2.0
1102		6	6	0	16	2.0
1103		5	5	0	16	2.0
1104		4	4	0	16	2.0
1105		3	3	0	16	2.0
1106		2	2	0	16	2.0
1107		1	1	0	16	2.0
1108	GAMMA	0	0	0	14	2.0
1109		1	0	0	14	2.0

```
                2    0    0   14  2.0
                3    0    0   14  2.0
                4    0    0   14  2.0
                5    0    0   14  2.0
                6    0    0   14  2.0
X               6    0    0   12  2.0
                6    0    1   12  2.0
                6    0    2   12  2.0
                6    0    3   12  2.0
                6    0    4   12  2.0
                6    0    5   12  2.0
U               7    0    7   14  2.0
                6    0    7   14  2.0
                5    0    7   14  2.0
                4    0    7   14  2.0
                3    0    7   14  2.0
                2    0    7   14  2.0
                1    0    7   14  2.0
Z               0    0    7   14  2.0
-------------------------------------------------------------------------
```

***Stishovite* and *Rutile*:**

```
GAMMA      0    0    0   22  2.0-8.00 8.00
           0    0    1   22  2.0
           0    0    2   22  2.0
           0    0    3   22  2.0
           0    0    4   22  2.0
LAMBDA     0    0    5   22  2.0
           0    0    6   22  2.0
           0    0    7   22  2.0
           0    0    8   22  2.0
           0    0    9   22  2.0
           0    0   10   22  2.0
Z          0    0   10   20  2.0
           1    1   10   20  2.0
           2    2   10   20  2.0
           3    3   10   20  2.0
           4    4   10   20  2.0
S          5    5   10   20  2.0
           6    6   10   20  2.0
           7    7   10   20  2.0
```

1152		8	8	10	20	2.0
1153		9	9	10	20	2.0
1154	A	11	11	11	22	2.0
1155		11	11	10	22	2.0
1156		11	11	9	22	2.0
1157		11	11	8	22	2.0
1158		11	11	7	22	2.0
1159	V	11	11	6	22	2.0
1160		11	11	5	22	2.0
1161		11	11	4	22	2.0
1162		11	11	3	22	2.0
1163		11	11	2	22	2.0
1164		11	11	1	22	2.0
1165	M	10	10	0	20	2.0
1166		9	9	0	20	2.0
1167		8	8	0	20	2.0
1168		7	7	0	20	2.0
1169		6	6	0	20	2.0
1170	SIGMA	5	5	0	20	2.0
1171		4	4	0	20	2.0
1172		3	3	0	20	2.0

1173		2	2	0	20	2.0
1174		1	1	0	20	2.0
1175	GAMMA	0	0	0	14	2.0
1176		1	0	0	14	2.0
1177		2	0	0	14	2.0
1178		3	0	0	14	2.0
1179	DELTA	4	0	0	14	2.0
1180		5	0	0	14	2.0
1181		6	0	0	14	2.0
1182	X	11	0	0	22	2.0
1183		11	0	1	22	2.0
1184		11	0	2	22	2.0
1185		11	0	3	22	2.0
1186		11	0	4	22	2.0
1187	W	11	0	5	22	2.0
1188		11	0	6	22	2.0
1189		11	0	7	22	2.0
1190		11	0	8	22	2.0
1191		11	0	9	22	2.0
1192		11	0	10	22	2.0
1193	R	7	0	7	14	2.0

```
                6    0    7   14  2.0
                5    0    7   14  2.0
                4    0    7   14  2.0
U               3    0    7   14  2.0
                2    0    7   14  2.0
                1    0    7   14  2.0
Z               0    0    7   14  2.0

-----------------------------------------------------------------------
```

***Coesite*:**

```
K.1             0    0    0 3822  2.0-8.00 8.00
                0  273    0 3822  2.0
                0  546    0 3822  2.0
                0  819    0 3822  2.0
                0 1092    0 3822  2.0
                0 1365    0 3822  2.0
                0 1638    0 3822  2.0
K.2             0 4095    0 8190  2.0
              183 4095  180 8190  2.0
              366 4095  360 8190  2.0
```

```
1215                549 4095  540 8190  2.0
1216                732 4095  720 8190  2.0
1217                915 4095  900 8190  2.0
1218               1098 4095 1080 8190  2.0
1219               1281 4095 1260 8190  2.0
1220               1464 4095 1440 8190  2.0
1221               1647 4095 1620 8190  2.0
1222               1830 4095 1800 8190  2.0
1223               2013 4095 1980 8190  2.0
1224               2196 4095 2160 8190  2.0
1225               2379 4095 2340 8190  2.0
1226               2562 4095 2520 8190  2.0
1227   K.3         1281 1911 1260 3822  2.0
1228               1281 1638 1260 3822  2.0
1229               1281 1365 1260 3822  2.0
1230               1281 1092 1260 3822  2.0
1231               1281  819 1260 3822  2.0
1232               1281  546 1260 3822  2.0
1233               1281  273 1260 3822  2.0
1234   K.4         2745    0 2700 8190  2.0
1235               2562    0 2520 8190  2.0
```

```
2379    0 2340 8190  2.0
2196    0 2160 8190  2.0
2013    0 1980 8190  2.0
1830    0 1800 8190  2.0
1647    0 1620 8190  2.0
1464    0 1440 8190  2.0
1281    0 1260 8190  2.0
1098    0 1080 8190  2.0
 915    0  900 8190  2.0
 732    0  720 8190  2.0
 549    0  540 8190  2.0
 366    0  360 8190  2.0
 183    0  180 8190  2.0
K.5       0    0    0 7098  2.0
 273    0    0 7098  2.0
 546    0    0 7098  2.0
 819    0    0 7098  2.0
1092    0    0 7098  2.0
1365    0    0 7098  2.0
1638    0    0 7098  2.0
1911    0    0 7098  2.0
```

```
1257              2184    0    0 7098  2.0
1258              2457    0    0 7098  2.0
1259              2730    0    0 7098  2.0
1260              3003    0    0 7098  2.0
1261              3276    0    0 7098  2.0
1262  K.6         1911    0    0 3822  2.0
1263              1911  273    0 3822  2.0
1264              1911  546    0 3822  2.0
1265              1911  819    0 3822  2.0
1266              1911 1092    0 3822  2.0
1267              1911 1365    0 3822  2.0
1268              1911 1638    0 3822  2.0
1269  K.7         3549 3549    0 7098  2.0
1270              3276 3549    0 7098  2.0
1271              3003 3549    0 7098  2.0
1272              2730 3549    0 7098  2.0
1273              2457 3549    0 7098  2.0
1274              2184 3549    0 7098  2.0
1275              1911 3549    0 7098  2.0
1276              1638 3549    0 7098  2.0
1277              1365 3549    0 7098  2.0
```

```
             1092 3549    0 7098  2.0
              819 3549    0 7098  2.0
              546 3549    0 7098  2.0
              273 3549    0 7098  2.0
K.8             0 3549    0 7098  2.0
```

APPENDIX 2 Comparison of band structures of *α-quartz* in the GW approximation (A2-1) and using the mBJ potential with spin polarization and self-interaction correction for the Si3d orbitals (A2-2). Experimental bandgap obtained by low-loss measurement in EELS/TEM is 9.65 eV from Garvie et al. (2000).

A2-1: GW method from Chang et al. (2000):

Figure A2-1

Figure A2-1. Calculated quasiparticle band structure of *α-quartz* in the GW approximation.

A2-2. Present mBJ method:

Figure A2-2

Figure A2-2. Calculated band structure of *α-quartz* in the mBJ/spin-polarized/Si3d-FLL approximation.

The two approaches yield very similar band structures of *α*-quartz and a very good account for the bandgap. Experimental gap energy is 9.65 eV, Γ→Γ gap is 10.1 eV calculated by the GW approximation and 9.41 eV in the present work using the mBJ approximation.

APPENDIX 3 Partial DOS in the VBs of *coesite, α-quartz, stishovite and seifertite.*

Partial DOS graphs presented here reveal the causes of occurrence of intra-VB gap in silica polymorphs with tetrahedrally coordinated Si. Figure A3-1 shows conditions prevailing in *coesite*, Figure A3-2 those in *α-quartz*, Figure A3-3 in *stishovite* and Figure A3-4 in *seifertite*.

Common features of the two tetrahedral polymorphs *coesite* and *α-quartz* are: (a) low contributions of Si to the split-off upper portion of VB; (b) significant contributions of Si to the split-off lower portion of VB; and (c) overlap of Si and O contributions in the lower VB indicating covalent Si-O bonding (Figures A3-1 and A3-2).

Figure A3-1

Figure A3-1 Partial VB DOS of Si and O contributions in *coesite*, showing a separation of ionic O2p band from covalent Si-O band across a 1.3 eV intrinsic gap.

Figure A3-2

Figure A3-2 Partial VB DOS of Si and O contributions in *α-quartz*, showing a separation of ionic O2p band from covalent Si-O band across a 1.7 eV intrinsic gap.

Common features of the two octahedral polymorphs *stishovite* and *seifertite* entail continuous, predominantly O2p valence bands with small, progressively decreasing contributions of Si from the bottom to the top of the VB (Figures A3-3 and A3-4).

Figure A3-3

Figure A3-3 Partial VB DOS of Si and O contributions in *stishovite*, showing a continuous band dominated by O2p orbitals with small contribution of Si orbitals decreasing from the bottom to the top of VB.

Figure A3-4

Figure A3-4 Partial VB DOS of Si and O contributions in *seifertite*, showing features similar to those of the *stishovite* VB in Figure A3-3.

1356

1357

1358

1359

1360

1361

1362

1363

1364

1365

1366

1367

1368

1369

1370

1371

1372

1373

FIGURES

Figures are presented in the following separate files:

"Optical absorption anisotropy of wide gap silica polymorphs stishovite – AmMiner-Figures-Revision1.docx", and

"Optical absorption anisotropy of wide gap silica polymorphs stishovite – AmMiner-Figures-Revision1.pdf".

TABLES

Table 1 Experimentally determined properties of silica polymorphs investigated here and of selected reference materials

SiO_2 polymorph	Density gm/cc	Refractive index at 0.588 nm	Mohs scale hardness	Space group	Optical bandgap eV	Si coordination
Seifertite [a,b]	4.294	n.a.	> 8	60 Pbcn	n.a.	$SiO_{2,2,2}$ [~octahedral]
Stishovite [c,d,e]	4.28-4.30	1.799 – 1.800 [n_ω] 1.826-1.845 [n_ε]	9 – 10	136 P42/mnm	8.75 – 7.6	$SiO_{4,2}$ [~octahedral]
Coesite [f,g,e]	2.911	n_x = 1.594 n_y = 1.595 n_z = 1.599	7.5	15 C2/c	8.6	SiO_4 [~tetrahedral]
Cristobalite [h,i]	2.33	1.487 [n_ω] 1.484 [n_ε]	6 - 7	92 $P4_12_12$ 227 Fd-3m	n.a.	SiO_4 [~tetrahedral]
Quartz [j]	2.65 -	1.54426	7	*α-quartz*:	9.65	SiO_4

	2.66			152 $P3_121$ and 154 $P3_221$ *β-quartz*: 180 $P6_222$ and 181 $P6_422$		[~tetrahedral]
$MgSiO_3$ *Ilmenite* [k]	2.4 – 2.7	2.40 – 2.42	5-6	148 R-3	n.a.	$SiO_{3,3}$ [~octahedral]
Amorphous silica [l,m]	2.648	1.458	n.a.	1 P1	8.0 – 9.3	SiO_4 [~tetrahedral]

[a] Dera et al. (2002); [b] El Goresy et al. (2008); [c] Stishov and Popova (1961); [d] Chao et al. (1962); [e] Trukhin et al. (2004); [f] Coes (1953); [g] Smyth et al. (1987);

[h] http://en.wikipedia.org/wiki/Cristobalite; [i] Experimental bandgaps are nearly independent for various silica polymorphs where available from the literature. However, theoretical bandgaps span a range of some 2 eV, from 8 to 10 eV (Ramos et al. 2004, present work);

[j] Garvie et al. (2000); [k] Horiuchi et al. (1982); [l] Vella et al. (2011); [m] Weinberg et al. (1979).

Table 2 Empirical bond-valence parameters R_0 and b, bond strength S, and bond covalence fraction f_c

Mineral	R (Å)	R_0 (Å)	b (Å)	S (v.u.from Eq.VI-1)	f_c (covalent fraction of M-O bond)
Seifertite	1.74158	1.624	0.37	0.72776	0.32067
Stishovite	1.75682	1.624	0.37	0.69839	0.29972
Rutile TiO_2	1.94323	1.815	0.37	0.70711	0.28438
Coesite [a]	1.59552 [a]	1.624	0.37	1.08001	0.61266
Coesite [b]	1.60536 [b]	1.624	0.37	1.05167	0.58651
α-Quartz	1.60146	1.624	0.37	1.06281	0.59674

[a] Shortest Si-O bond distance in *coesite*

[b] Longest Si-O bond distance in *coesite*

Table 3 Effective mass m_{eff} in *seifertite, stishovite, coesite* and *rutile* in units of electron mass m_e = 9.10938e-31 kg.

m_{eff}	*seifertite*	*stishovite*	*coesite*	TiO_2 *rutile*
CBM at Γ-point, z-direction	0.434	0.433	0.550 [a]	0.789
CBM at Γ-point, x-direction	0.452	0.541	0.553	0.923 [b]
VBM at Γ-point, z-direction	5.551	1.823	4.549	3.737
VBM at Γ-point, x-direction	0.492	1.127	2.551	2.172
Bandgap. eV	7.49608	7.57373	8.52257	3.116 [c]

[a] z-direction in *coesite* is approximate due to its monoclinic structure

[b] M→A direction

[c] Ti3d U_{eff} = 0.25 was chosen as in Solovyev, Dederichs and Anisimov (1994)

This is a preprint, the final version is subject to change, of the American Mineralogist (MSA)
Cite as Authors (Year) Title. American Mineralogist, in press.
(DOI will not work until issue is live.) DOI: http://dx.doi.org/10.2138/am-2015-4890

Optical absorption anisotropy of high-density, wide-gap, high-hardness SiO_2 polymorphs *seifertite*, *stishovite* and *coesite*.

Kamil Klier[a], Jeffery A. Spirko[b] and Kai M. Landskron[a]

[a] Department of Chemistry, Lehigh University, E. Packer Ave, Bethlehem, PA 18015
[b] Department of Physical and Environmental Sciences, Texas A&M University-Corpus Christi, 6300 Ocean Dr, Unit 5802, Corpus Christi, TX 78414-58

FIGURES

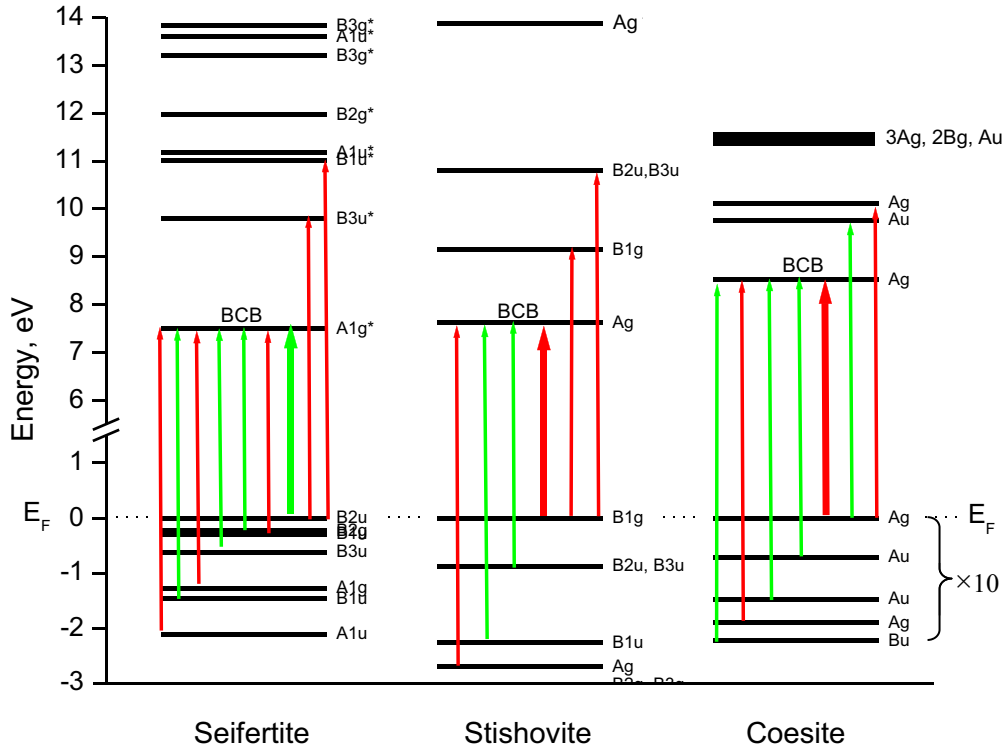

Figure 1. Band-to-band transitions at the Γ-points of the BZ at the direct gaps of (a) *seifertite* (using Mulliken irreducible representation labels of the D_{2h} group), (b) *stishovite* (D_{2h}) and (c) *coesite* (C_{2h}). Green (red) arrows mark electric dipole allowed (forbidden) transitions. Thick arrows represent transitions VBM ($E_F = 0$) → CBM which are allowed in *seifertite*, and forbidden in *stishovite* and *coesite*. The closely separated valence band levels in *coesite* are expanded for clarity. The symbol for the bottom of conduction band BCB is used interchangeably with CBM.

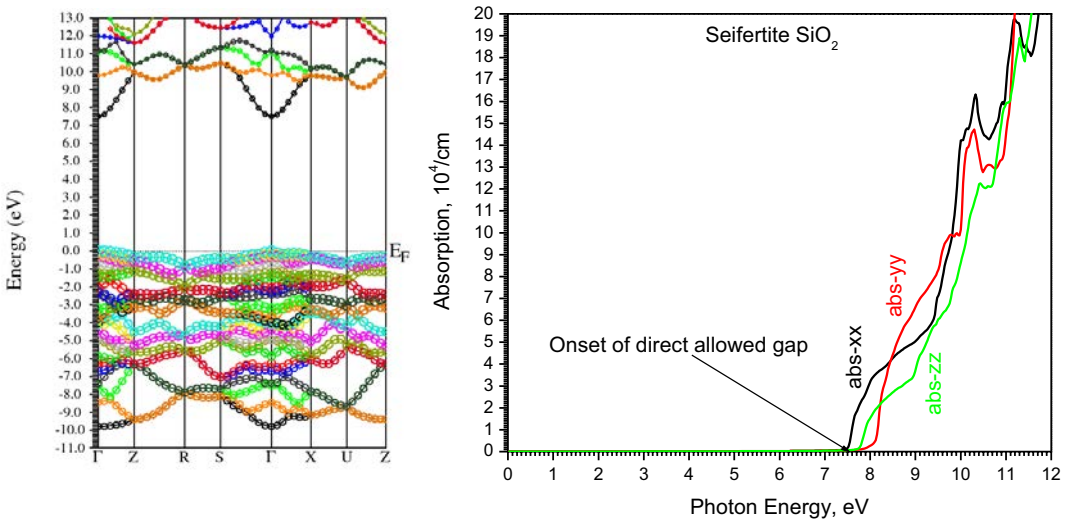

Figure 2. Band structure and optical absorption of ***seifertite***

Left – Energy band structure in the momentum space. Symbols for special points of the Brillouin zone are given in caption to Figure A1-2 in Appendix 1. Sizes of heavier plotting are given in parentheses with O2p-orbitals emphasized (0.2). Character of the bottom of conduction band (BCB) is a mixture of Si s-orbitals and a symmetric combination of O p-orbitals to give the total state symmetry A_g. The top of the valence band (TVB) is an antisymmetric combination of O2p orbitals of total state symmetry B_{2u}, giving rise to allowed TVB (B_{2u}) → BCB (A_g) transition.

Right – Optical absorption spectra along the principal crystallographic axes of the orthorhombic structure. Allowed lowest transition across the direct bandgap gives rise to a sharp band edge at 7.5 eV excited by the y- (B_{2u}) component of the light electric dipole.

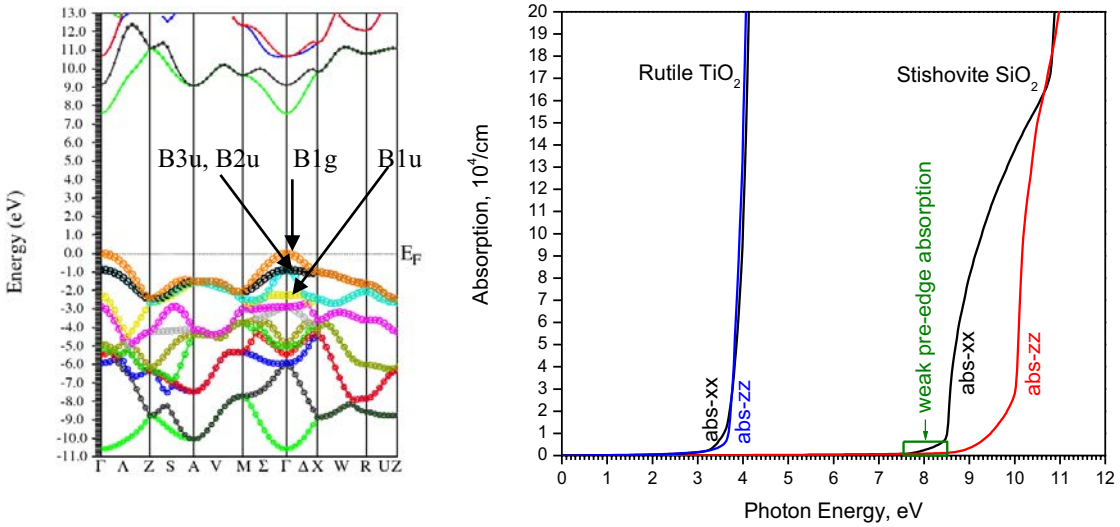

Figure 3. Band structure and optical absorption of ***stishovite***

Left - Energy band structure in the momentum space. Symbols for special points of the Brillouin zone are given in caption to Figure A1-4 in Appendix 1. Sizes of heavier plotting are given in parentheses with O2p-orbitals emphasized (0.2). Character of CBM is mainly Si s-orbitals (not emphasized) of total state symmetry A_g under the D_{2h} group. The VBM is a combination of O2p orbitals to give total state symmetry B_{1g} and the VBM (B_{1g}) → CBM (A_g) transition is symmetry and parity forbidden. Details of splitting of O2p orbitals near VBM are indicated by arrows and symmetry labels. Transitions from B_{3u}, B_{2u} and B_{1u} VB states to A_g (CBM) are allowed by the x,y- (B_{3u},B_{2u}) and z- (B_{1u}) components of electric dipole.

Right - Optical absorption spectra of *stishovite* along the principal crystallographic axes of the tetragonal structure showing a pre-edge absorption and a large anisotropy between equatorial (abs-xx = abs-yy) and apical (abs-zz) absorptions. Spectra of the isostructural *rutile* lacking such an anisotropy are shown for comparison.

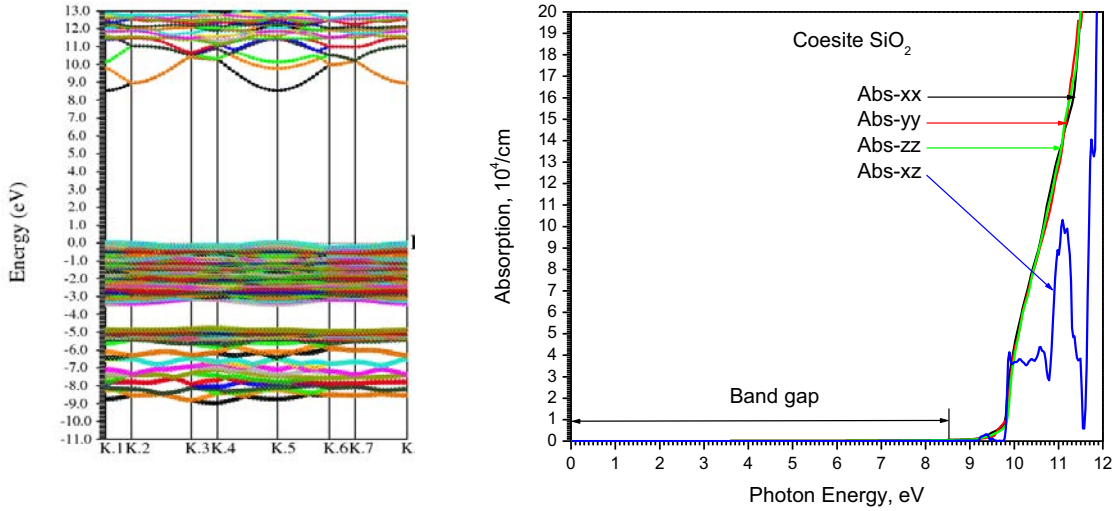

Figure 4. Band structure and optical absorption of ***coesite***.

Left - With O orbitals emphasized (0.4). Labels of the BZ special points are specified in Figure A1-6 in Appendix 1.

Right - Optical absorption spectra of *coesite* along the principal crystallographic axes of the monoclinic structure (Abs-xx, -yy, -zz) and off-diagonal Abs-xz.

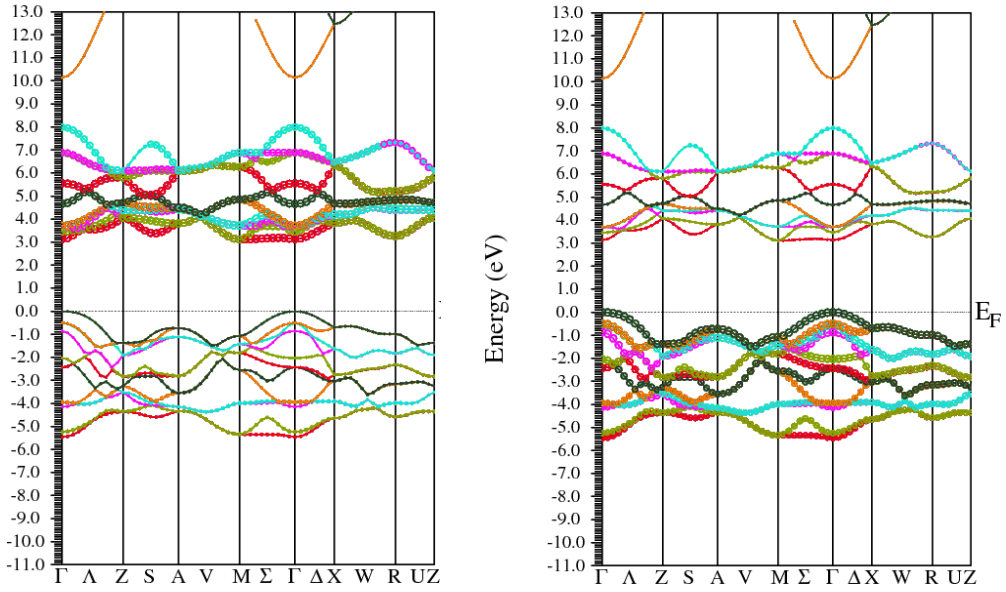

Figure 5. Band structure of TiO_2 ***rutile***.

Left - with Ti3d orbitals emphasized;

Right - with O2p orbitals emphasized.

Symbols for special points of the BZ are given in caption to Figure A1-4 in Appendix 1 and their layout is identical with that of the isostructural *stishovite* (Figure 3) for comparison.

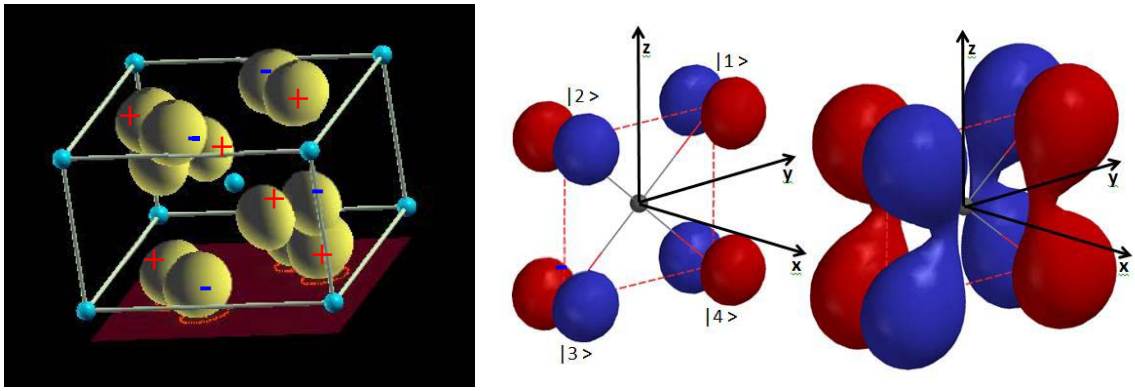

Figure 6 Representation of the O2p – based orbitals of *stishovite* that give rise to the B_{1g} state at the TVB.

Left: calculated MO density at the Γ-point to within 0.1 eV from the Fermi level, showing the p-character of the orbitals of six O ligands around the central Si atom (cf. Figure A1-3 of Appendix 1). Corresponding phases of the wavefunction are marked with + and – signs.

Center: Schematic representation of the B_{1g} crystal orbital at the VBM. For a clear symmetry analysis, the x-axis is chosen as normal to the (110) plane (dashed outline) and the y-axis is placed in the (110) plane, i.e. in directions rotated about the crystallographic z-axis by 45°, while the z-axis coincides with the crystallographic z-direction of Figure 3 of Appendix 1. Phases of the equatorial $O2p_x$ orbitals are color coded red (+) and blue (-). Atomic $O2p_x$ orbitals form a 4-dimensional reducible representation Γ_4 which is reduced, using projection operators of the D_{2h} group, as $\Gamma_4 = B_{1g} \oplus B_{1u} \oplus B_{2u} \oplus B_{3u}$. The B_{1g} state is realized by the combination $|B_{1g}> = N [|1> - |2> - |3> + |4>]$ as depicted in the center panel. Apical $O2p_y$ orbitals on the x-axis (shown only in the left panel) are in antibonding relation to the equatorial set and conform to the B_{1g} symmetry.

Right: An overlap between equatorial orbitals $|1> + |4>$, and $|2> + |3>$, and a node between these two sets results in a weak π-bonding that is topologically equivalent to that in HOMO of cyclobutadiene. Thus the B_{1g} symmetry of the O2p VBM originates from the planar rectangular cyclical structure of oxygen "ligands" to the Si atom.

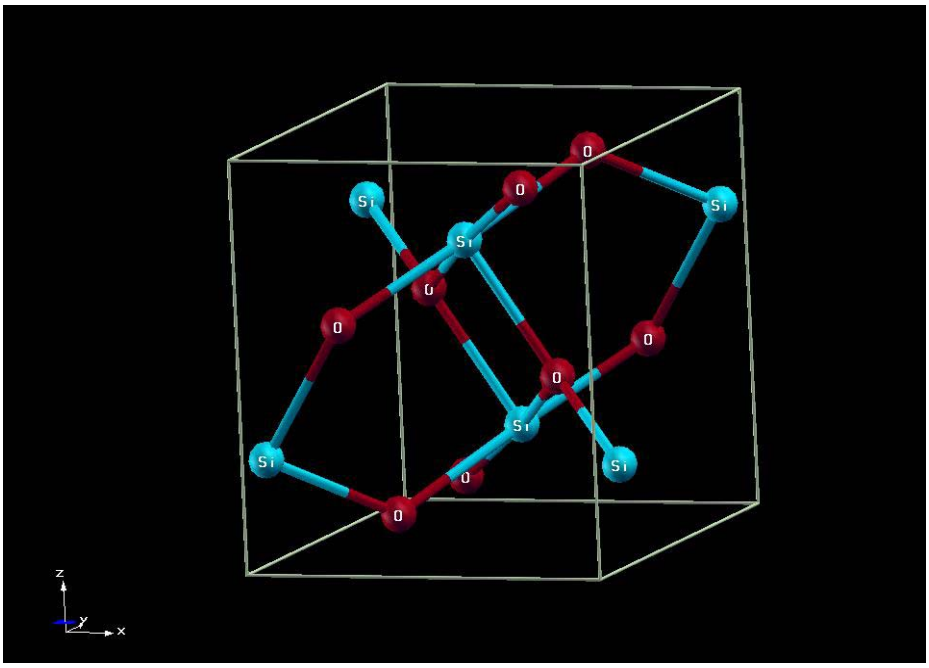

Figure A1-1 Unit cell of *seifertite.* Values of primitive translations **a**, **b**, **c** in the x, y, z directions and fractional coordinates of Si and O are given in the text. The coordination of Si by O is nearly octahedral and that of O by Si is trigonal.

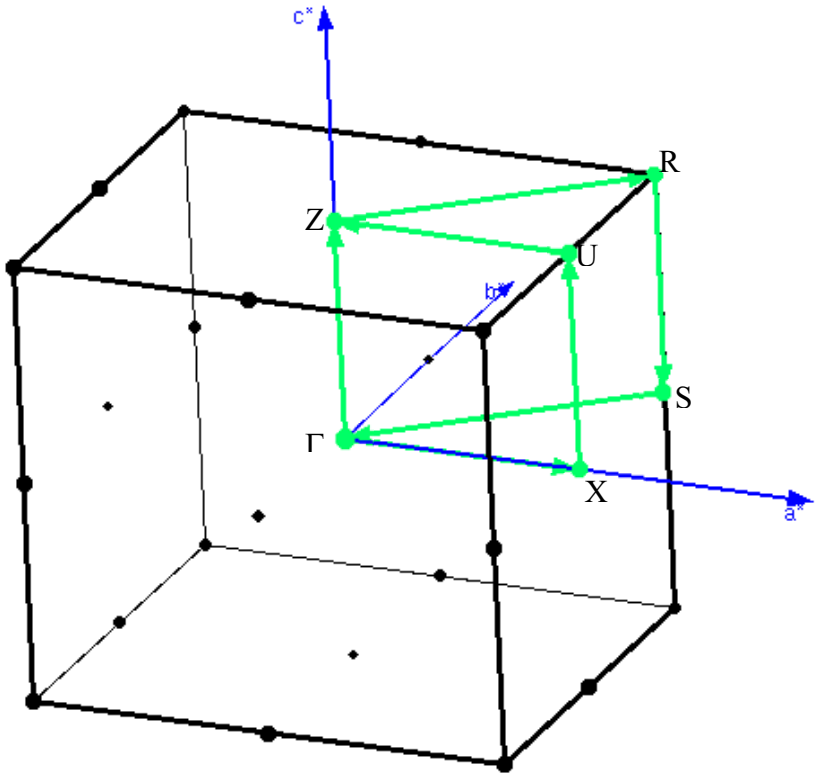

Figure A1-2 Brillouin zone of the orthorhombic lattice. Critical points chosen for the band structure representation are labeled as Γ (0,0,0), Z (0,0, ½), R (½, ½, ½), S (½, ½,0), X (½,0,0), U (½,0, ½). Lengths of the reciprocal vectors **a***, **b***, **c*** are in the ratio generated by the *seifertite* structure.

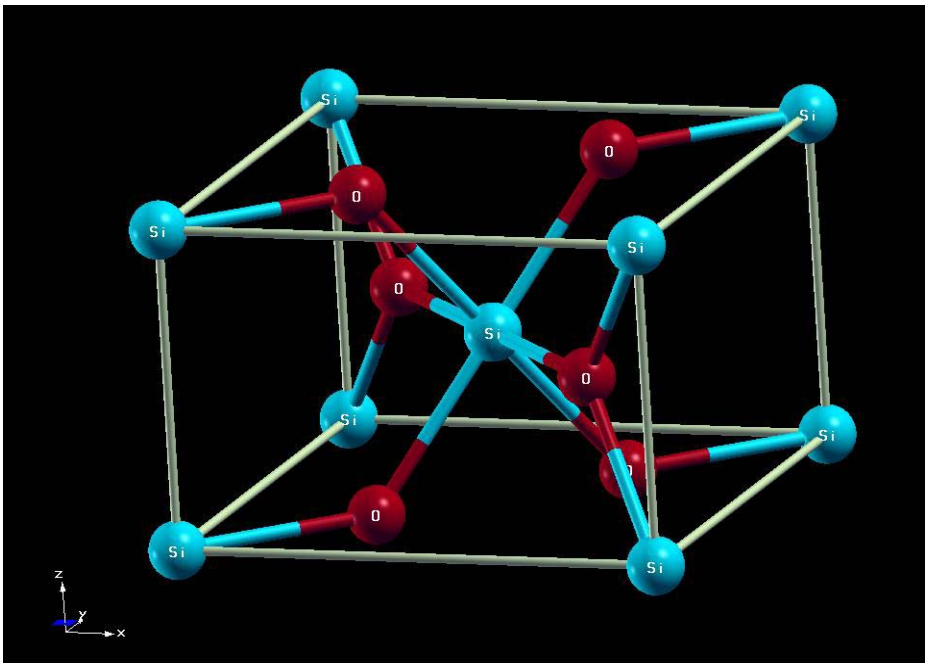

Figure A1-3 Unit cell of *stishovite.* Values of primitive translations **a**, **b**, **c** in the x, y, z directions and fractional coordinates of Si and O are given in the text. The coordination of Si by O is nearly octahedral and that of O by Si is trigonal.

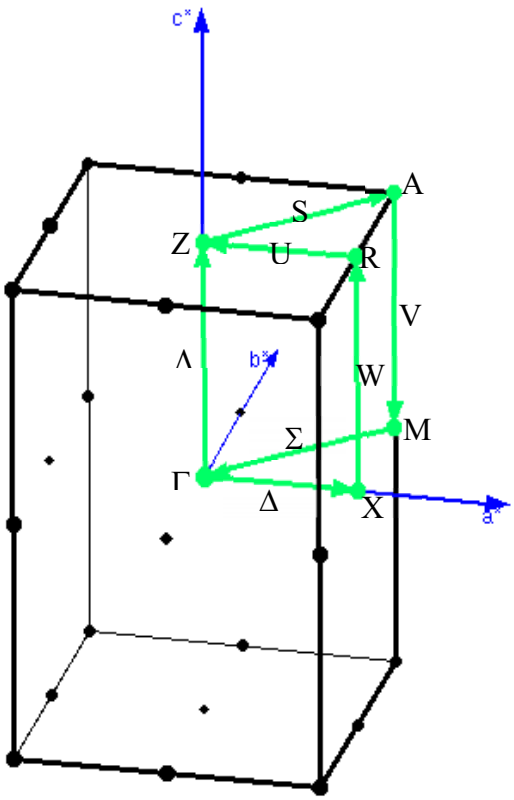

Figure A1-4 Brillouin zone of the tetragonal lattice. Critical points chosen for the band structure representation are labeled as Γ (0,0,0), Z (0,0, ½), A (½, ½, ½), M (½, ½,0), X (½,0,0), R (½,0, ½). Intermediate points Λ, S, V, Σ, Δ, W and U have coordinates specified in the klist_band for the tetragonal lattice. Lengths of the reciprocal vectors **a***, **b***, **c*** are in the ratio yielded by the *stishovite* structure.

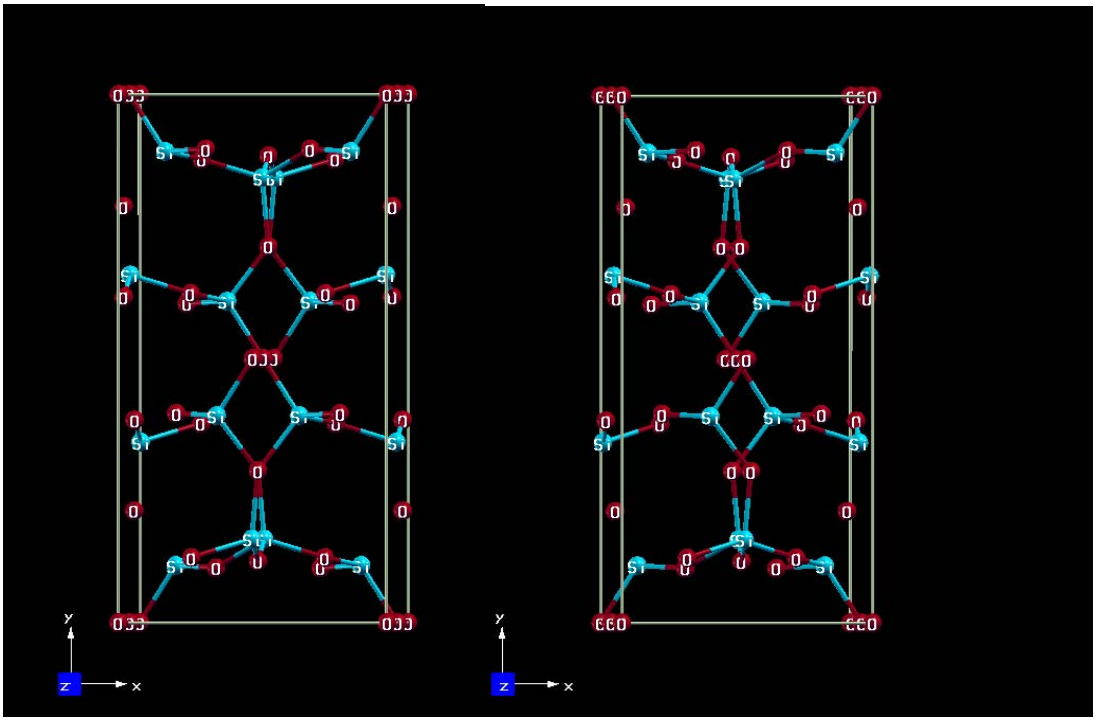

Figure A1-5 Unit cell of *coesite* as a stereo picture. Values of primitive translations **a**, **b**, **c** in the x, y, z directions and fractional coordinates of Si and O are given in the text. The coordination of Si by O is tetrahedral and that of O by Si is two-fold. O atoms at (0,0,0) and (1/2,1/2,1/2) are linearly coordinated to the nearest two Si neighbors, a feature that has influence on distribution of levels in the valence band.

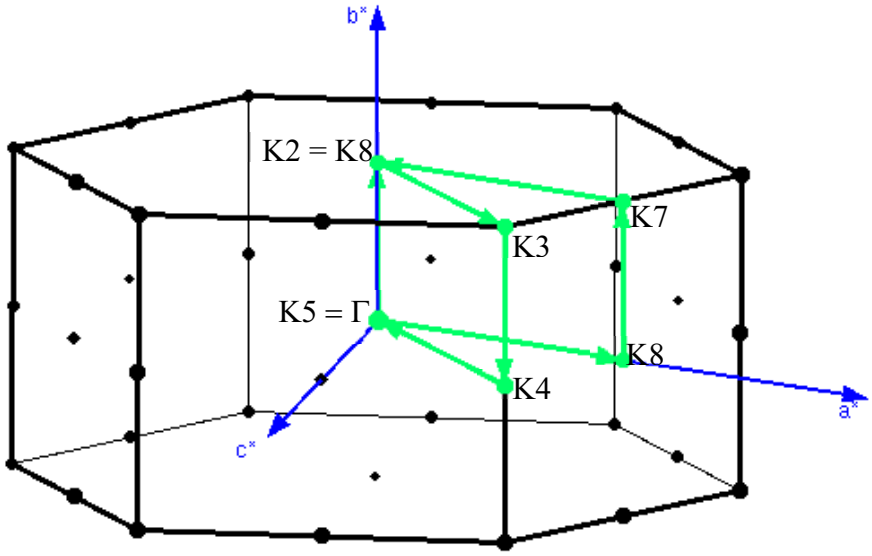

Figure A1-6 Brillouin zone of the monoclinic, nearly hexagonal lattice about the **b*** axis. Critical points chosen for the band structure representation are labeled as:
Γ (0,0,0), K2 (0, ½, 0), K3 (0.335, ½, 0.33), K4 (0.335,0, 0.33), K5 = Γ, K6 (½,0,0), K7 (½,½,0), K8 = K2.
The corresponding labels for the idealized hexagonal lattice are:
Γ ≡ [K1 = K5], A ≡ [K2 = K8], H ≡ K3, K ≡ K4, M ≡ K6 and L ≡ K7.
The lengths of and angles between the reciprocal vectors **a***, **b***, **c*** are in the ratio created by the *coesite* structure.

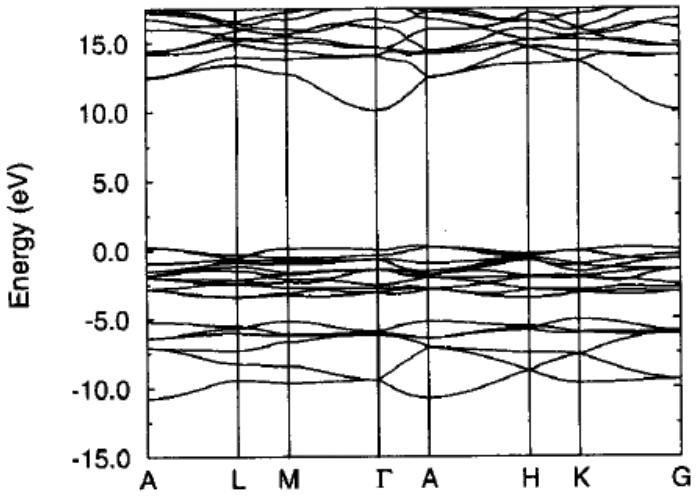

Figure A2-1. Calculated quasiparticle band structure of *α-quartz* in the GW approximation.

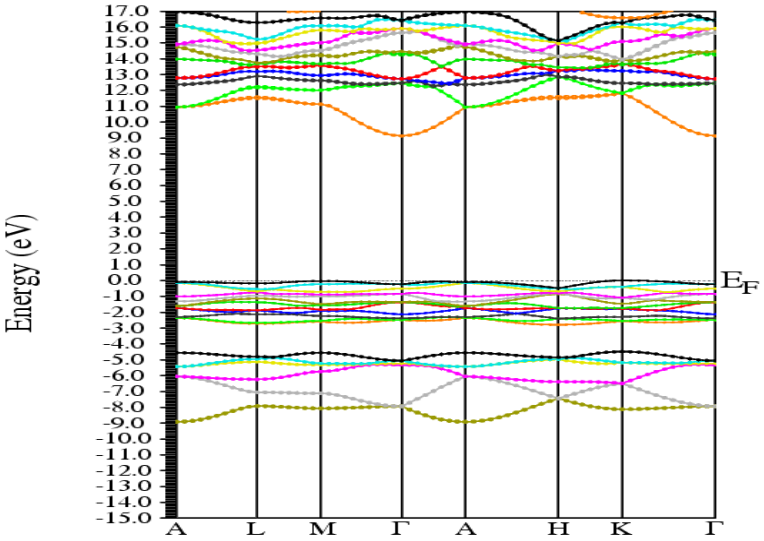

Figure A2-2. Calculated band structure of *α-quartz* in the mBJ/spin-polarized/Si3d-SIC approximation.

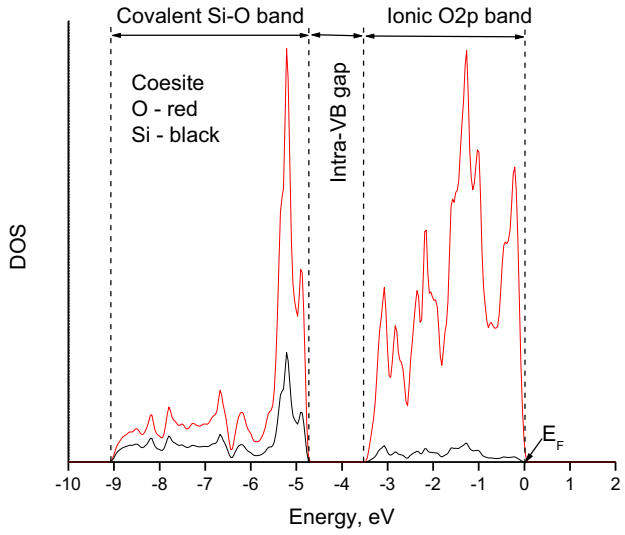

Figure A3-1. Partial VB DOS of Si and O contributions in *coesite*, showing a separation of ionic O2p band from covalent Si-O band across a 1.3 eV intrinsic gap.

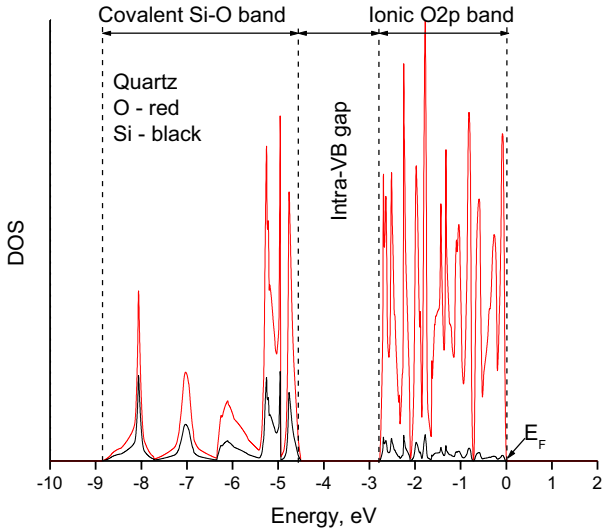

Figure A3-2. Partial VB DOS of Si and O contributions in *α-quartz*, showing a separation of ionic O2p band from covalent Si-O band across a 1.7 eV intrinsic gap. Common features of the two tetrahedral polymorphs *coesite* and *α-quartz* are: (a) low contributions of Si to the split-off upper portion of VB; (b) significant contributions of Si to the split-off lower portion of VB; and (c) overlap of Si and O contributions in the lower VB indicating covalent Si-O bonding.

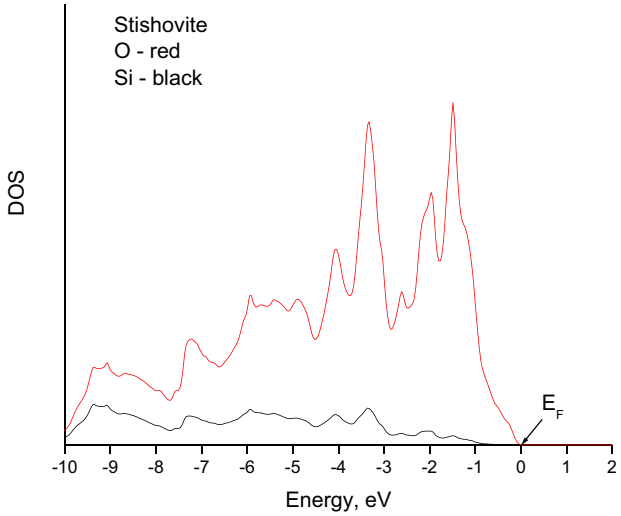

Figure A3-3. Partial VB DOS of Si and O contributions in *stishovite*, showing a continuous band dominated by O2p orbitals with small contribution of Si orbitals decreasing from the bottom to the top of VB.

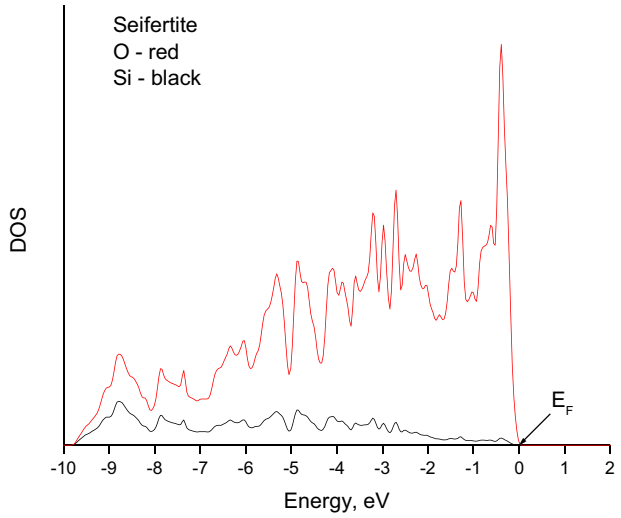

Figure A3-4. Partial VB DOS of Si and O contributions in *seifertite*, showing features similar to those of the *stishovite* VB in Figure A3-3.

Common features of the two octahedral polymorphs *stishovite* and *seifertite* entail continuous, predominantly O2p valence bands with small, progressively decreasing contributions of Si from the bottom to the top of the VB.

Optical absorption anisotropy of high-density, wide-gap, high-hardness SiO_2 polymorphs *seifertite*, *stishovite* and *coesite*.

Kamil Klier[a], Jeffery A. Spirko[b], and Kai M. Landskron[a]

TABLES

Table 1 Experimentally determined properties of silica polymorphs and selected reference materials

SiO_2 polymorph	Density (gm/cc)	Refractive index at 0.588 nm	Mohs scale hardness	Space group	Optical bandgap (eV)	Si coordination
Seifertite [a,b]	4.294	n.a.	> 8	60 Pbcn	n.a.	$SiO_{2,2,2}$ [~octahedral]
Stishovite [c,d,e]	4.28-4.30	1.799 – 1.800 [n_ω] 1.826-1.845 [n_ε]	9 – 10	136 P42/mnm	8.75 – 7.6	$SiO_{4,2}$ [~octahedral]
Coesite [f,g,e]	2.911	$n_x = 1.594$ $n_y = 1.595$ $n_z = 1.599$	7.5	15 C2/c	8.6	SiO_4 [~tetrahedral]
Cristobalite [h,i]	2.33	1.487 [n_ω] 1.484 [n_ε]	6 - 7	92 $P4_12_12$ 227 Fd-3m	n.a.	SiO_4 [~tetrahedral]
Quartz [j]	2.65 - 2.66	1.54426	7	*α-quartz*: 152 $P3_121$ and 154 $P3_221$ *β-quartz*: 180 $P6_222$ and 181 $P6_422$	9.65	SiO_4 [~tetrahedral]
$MgSiO_3$ *Ilmenite* [k]	2.4 – 2.7	2.40 – 2.42	5-6	148 R-3	n.a.	$SiO_{3,3}$ [~octahedral]
Amorphous silica [l,m]	2.648	1.458	n.a.	1 P1	8.0 – 9.3	SiO_4 [~tetrahedral]

Notes: [a] Dera et al. (2002). [b] El Goresy et al. (2008). [c] Stishov and Popova (1961). [d] Chao et al. (1962). [e] Trukhin et al. (2004). [f] Coes (1953). [g] Smyth et al. (1987). [h] http://en.wikipedia.org/wiki/Cristobalite. [i] Experimental bandgaps are nearly independent for various silica polymorphs where available from the literature. However, theoretical bandgaps span a range of some 2 eV, from 8 to 10 eV (Ramos et al. 2004, present work). [j] Garvie et al. (2000). [k] Horiuchi et al. (1982). [l] Vella et al. (2011). [m] Weinberg et al. (1979).

Table 2 Empirical bond-valence parameters R_0 and b, bond strength S, and bond covalence fraction f_c

Mineral	**R** (Å)	$\mathbf{R_0}$ (Å)	**b** (Å)	**S** (v.u.from Eq.VI-1)	$\mathbf{f_c}$ (covalent fraction of M-O bond)
Seifertite	1.74158	1.624	0.37	0.72776	0.32067
Stishovite	1.75682	1.624	0.37	0.69839	0.29972
Rutile TiO_2	1.94323	1.815	0.37	0.70711	0.28438
Coesite [a]	1.59552 [a]	1.624	0.37	1.08001	0.61266
Coesite [b]	1.60536 [b]	1.624	0.37	1.05167	0.58651
α-Quartz	1.60146	1.624	0.37	1.06281	0.59674

Notes: [a] Shortest Si-O bond distance in *coesite.* [b] Longest Si-O bond distance in *coesite.*

Table 3 Effective mass m_{eff} in seifertite, stishovite, coesite and rutile in units of electron mass m_e = 9.10938e-31 kg, and bandgap at the Γ-point

$\mathbf{m_{eff}}$	**seifertite**	**stishovite**	**coesite**	**TiO_2 rutile**
CBM at Γ-point, z-direction	0.434	0.433	0.550 [a]	0.789
CBM at Γ-point, x-direction	0.452	0.541	0.553	0.923 [b]
VBM at Γ-point, z-direction	5.551	1.823	4.549	3.737
VBM at Γ-point, x-direction	0.492	1.127	2.551	2.172
Bandgap (eV) [d]	7.49608	7.57373	8.52257	3.116 [c]

Notes: [a] z-direction in *coesite* is approximate due to its monoclinic structure. [b] M→A direction. [c] Ti3d U_{eff} = 0.25 was chosen as in Solovyev, Dederichs and Anisimov (1994). [d] Bandgap between valence band maximum (VBM) and conduction band minimum (CBM).